THE ASTROPHYSICAL JOURNAL, 300:675–697, 1986 January 15

THE CYGNUS LOOP: A DETAILED COMPARISON OF X-RAY AND OPTICAL EMISSION

J. JEFF HESTER[1,2] AND DONALD P. COX[1,3]
Received 1985 January 24; accepted 1985 July 17

ABSTRACT

A comparison is presented between X-ray and optical emission for a field on the southeast edge of the Cygnus Loop supernova remnant (SNR) using *Einstein* high-resolution imager (HRI) and narrow-band image-tube data. The two brightest regions of X-ray emission in the field are associated with optical emission. The edge of the brightest X-ray feature is coincident with the leading edge of the optical emission over a length of several minutes of arc. The spatial relationship is consistent with a thin ($\lesssim$0.2 pc) zone of enhanced X-ray emission lying immediately behind the much thinner sheet of optical emission. The interstellar medium (ISM) around the Cygnus Loop seems to consist of large (>1 pc) clouds surrounded by envelopes which are somewhat more dense than the rest of the intercloud medium. The data do not support the view that optical filaments are composed of myriads of tiny (<0.01 pc) cloudlets. Neither do the data suggest that the clouds containing the bright optical filaments have in general been engulfed by the blast wave. Evaporation as a means of enhancing X-ray emission is discussed and found to have a number of difficulties. A higher density intercloud medium in the vicinity of dense clouds and additional compression of the already shocked hot plasma behind the blast wave seem better able to account for the observations. The additional compression of the hot plasma could arise as a result of rapid deceleration of the blast wave and reflected or bow shocks around dense clouds. The Cygnus Loop does not appear to be an evaporative SNR expanding into a medium dominated by a coronal gas phase.

Subject headings: nebulae: individual — nebulae: supernova remnants — shock waves — X-rays: sources — interstellar: matter

I. INTRODUCTION

Its proximity, large apparent size, and high surface brightness have made the Cygnus Loop (the Veil Nebula, NGC 6960, NGC 6979, NGC 6992/5) a favored object for study of adolescent to middle-aged supernova remnants (SNRs). At a distance of roughly 770 pc (Minkowski 1958) the 3° diameter of the Loop corresponds to 40 pc at a scale of 1.15×10^{16} cm arcsec^{-1}. At this scale it is possible to study the optical structure of the Loop at a resolution approaching the scale of the stratification of the cooling and recombination zones responsible for the optical emission. (The reader is referred in particular to two recent optical studies [Fesen, Blair, and Kirshner 1982; Hester, Parker, and Dufour 1983, hereafter HPD] for descriptions and differing interpretations of the Loop.) It has also been possible to discern a great deal of the X-ray structure of the Loop, even using instruments with relatively poor spatial resolution (e.g., Rappaport *et al.* 1974, 1979). Most recently the Cygnus Loop was studied by Ku *et al.* (1984, hereafter KKPL), using the X-ray imaging systems aboard the *Einstein Observatory*. These studies have found that a gross correlation exists between the portions of the shell which are bright in X-rays and the large regions of filamentary emission which define the remnant optically.

The general picture of the Cygnus Loop which has evolved over the past 15 years is that of a middle-aged ($\sim$16,000 year old) supernova remnant still in the adiabatic phase of its evolution. The X-ray emission from the remnant is consistent with thermal emission behind a 300–400 km s^{-1} blast wave propagating into a medium of density 0.1–1 cm^{-3}, while the optical emission is due primarily to radiative shocks with velocities of $\sim$100 km s^{-1} being driven into clouds of density 2–10 cm^{-3}. While this basic picture (first put forward by McKee and Cowie 1975) seems fairly secure (see Falle and Garlick 1982 for a dissenting view), there are a number of pertinent questions upon which there is no general consensus. These questions deal, for example, with the size of clouds in the ambient medium, the applicability of steady flow shock calculations to optical and UV spectra, the three-dimensional structure of filaments, and the reason for the large-scale correlation of optical and X-ray emission.

In the present paper we present a comparison with a spatial resolution of 17″ (2×10^{17} cm = 0.06 pc, high by X-ray standards) between optical and X-ray emission from an 18′ diameter field on the southeast[4] edge of the Cygnus Loop, using data previously published by HPD and KKPL. In § II we present the data. In § III we describe the relationship between optical and X-ray emission in the field, generalizing to the Loop as a whole when possible. In § IV several possible explanations for the presence of bright X-ray emission in the vicinity of optical emission are presented and evaluated within the context of the data. These mechanisms involve evaporation, gradual variations and gradients in the density of the preshock intercloud medium, and additional compression of material which has already been heated to X-ray temperatures

[1] Department of Space Physics and Astronomy, Rice University.
[2] Visiting Student, Kitt Peak National Observatory, National Optical Astronomy Observatories, operated by the Association of Universities for Research in Astronomy, Inc., under contract with the National Science Foundation.
[3] On leave from the Department of Physics, University of Wisconsin at Madison.

[4] This region of the Cygnus Loop (NGC 6995) has traditionally been referred to as the "southeast" on the basis of its position at the southern end of the optically bright eastern limb. While this field lies almost due east of the center of the Loop as defined by the X-ray emission, we maintain the earlier nomenclature.

by the adiabatic blast wave. The additional compression could result from rapid deceleration of the blast wave itself or from reshocking by reflected or bow shocks around dense clouds. Section IV also addresses implications of the observations for models of SNR evolution and the interstellar medium (ISM).

II. DATA

Optical and X-ray imagery are presented for a field $\sim 18'$ in diameter located on the southeast edge of the Cygnus Loop. The optical data consist of [O III] λ5007 and [S II] λ6725 rasters generated from image-tube plates taken at f/7.5 using the No. 1, 91 cm telescope at Kitt Peak National Observatory. The plates were digitized using a PDS microdensitometer at KPNO and further reduced using the Rice University picture processing system. The data are a subset of those presented by HPD, where the optical morphology and spectral characteristics of the north-central part of the field are discussed in detail. These two emission lines were chosen for comparison with the X-ray data because they represent emission from the hottest and coolest parts of cooling and recombination regions behind radiative shocks.

Two overlapping X-ray images of this field obtained using the high-resolution imager (HRI) aboard the *Einstein Observatory* were graciously provided by William Ku of the Columbia Astrophysics Laboratory. These were among the data discussed by KKPL. The net observation times for the two images were 5806 and 5142 s. The two frames were normalized according to their exposure times, and a vignetting correction was applied to each assuming a 30% correction at 10′ off axis. The two were aligned using the field centers and scales supplied with each frame, transformed to the same "plate scale" as the optical rasters, then combined to form a mosaic which overlies the optical data directly. The X-ray raster is about 19′ on a side and contains the circular optical field.

The alignment of the optical data was based on positions for 70 stars in the field and 25 nearby SAO stars measured from a Palomar Schmidt plate. The relative alignment between the two optical rasters is good to 0.″3. On the basis of the errors in a fit to the star positions measured from the Schmidt plate, we find the overall uncertainty in the absolute alignment across the face of the optical rasters (due to uncorrected image-tube and telescope distortion) to be less than 3″. The uncertainty in pointing of the HRI is $\sim 10''$. The HRI has a nominal resolution of about 4″. It was necessary to smooth the X-ray data by convolution with a 17″ FWHM Gaussian before relatively clean surface brightness contours began to emerge from the counting statistics.

Figure 1 shows a linear gray scale map of the composite X-ray image. The faintest regions in the field have a surface brightness of ~ 0.01 counts arcmin^{-2} s^{-1}. The brightest knot has a surface brightness of ~ 0.17 counts arcmin^{-2} s^{-1}. North is at the top of the figure, and east is to the left. Figure 2 shows the optical data after suppression of the bright star centers. The signal-to-noise ratio of the data has been improved by rejecting pixels more than 2 σ from the mean of the surrounding 3 × 3 pixel window. The images have a resolution of $\sim 3''$. Figure 3 shows logarithmic contours of the smoothed optical data overlaid on the X-ray image. In order to facilitate comparisons with the X-ray data, the optical images were also smoothed to a FWHM of 17″ before generation of contours. The contour levels are separated by a factor of 2 in each case.

The most detailed and complete X-ray map of the Cygnus Loop to date (made by merging 59 *Einstein* IPC images) has recently been published by KKPL. In their Figure 1 they present this map overlaid on a Palomar Observatory Sky Survey (POSS) image of the Loop. Frequent reference is made to this map in the remainder of the present article, and the reader is advised to have a copy on hand. A color-coded version of their map appears in Henbest and Marten (1983, p. 201).

III. OPTICAL/X-RAY COMPARISONS

a) Overview of the Cygnus Loop

The general appearance of the Cygnus Loop at X-ray wavelengths has been discussed at length by KKPL. The basic appearance is that of a shell in which limb brightening is apparent around the entire circumference. In a limb-brightened shell geometry the scale over which the surface brightness drops off at the edge of the shell gives an estimate of the thickness of the emitting zone. From the radial profiles and composite IPC map in KKPL we estimate a thickness of order 1 pc for the zone of generally bright X-ray emission behind the adiabatic blast wave. The limb brightening is far from uniform, however. In some directions around the Loop the limb brightening is less than a factor of 2, whereas the contrast between the brightest features on the limb and the faintest regions interior to the Loop is a factor of 50. From the radial profiles and IPC map presented by KKPL it can be seen that much of the limb-brightened appearance is attributable to emission associated with optical features on the east and west limbs of the Loop. (Similar associations between the X-ray and the optical emission have been reported for other remnants. See, for example, Mathewson *et al.* 1983 for optical and IPC images of SNRs in the Magellanic Clouds.) The X-ray enhancements on the east and west limbs extend about 30′ further around the perimeter of the Loop than do the regions of optical emission with which they are associated. They also extend further toward the center of the Loop. These appear to be large flat regions ("pancakes") with the brightest X-ray emission and the optical emission in the center and fainter X-ray emission toward the edges.

Along the X-ray bright north-northeast limb of the Loop there are no bright optical filaments near the rim, although even here the X-ray emission is not completely without association with optical features. The northeast X-ray limb appears to be part of the extended pancake of emission centered on the optically bright east rim, and the bright X-ray emission along the north of the Loop extends toward the center far enough to encompass the region of optical emission at $\alpha = 20^{h}49^{m}$ and $\delta = 31°45'$. (Unfortunately, the IPC map is incomplete in this region, so the details of the association of the X-ray and optical emission are unknown.) The irregularity of the shell and the large-scale correlation between X-ray and optical emission emphasize that fits of the total X-ray luminosity of the Cygnus Loop to a Sedov (1959) model (e.g., Tucker 1971; KKPL) give only a rough idea of the average conditions around the Loop. Some direct evidence exists to suggest in particular that the density behind the blast wave in the X-ray bright regions is higher than average. Woodgate, Kirshner, and Balon (1977) used their [Fe XIV] measurements to infer a preshock density of 1 cm^{-3} for the northeast limb. As expected from the X-ray appearance, this is considerably higher than the overall rms value of 0.16 cm^{-3} obtained by Tucker and KKPL.

Deviations from circularity around the edge of the Loop are significant. The most striking departure from circularity is the

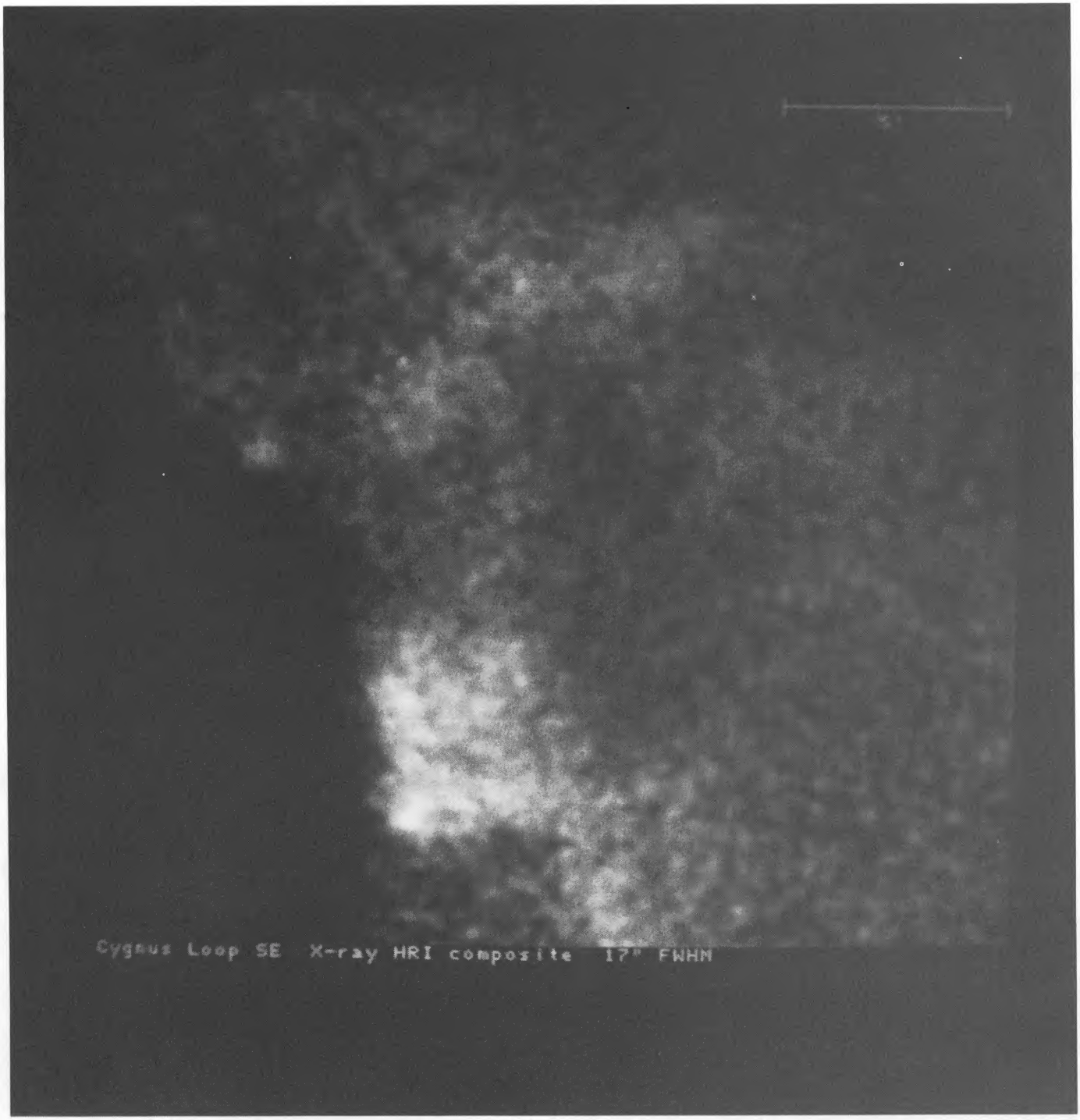

FIG. 1.—Linear gray scale map of the soft X-ray emission from a field on the southeast edge of the Cygnus Loop. The map is a composite of two *Einstein* HRI images provided by William Ku. The data have been smoothed by convolution with a Gaussian with FWHM = 17″ in order to generate relatively smooth surface brightness contours from the counting statistics of the HRI data. The brightest knot has a surface brightness of 0.17 counts arcmin^{-2} s^{-1}. The faintest regions on the east side of the field have an average surface brightness of 0.01 counts arcmin^{-2} s^{-1}.

"breakout" in the south, which has been interpreted as a direction of much lower than average preshock density. Apart from the breakout, the Loop could be described as "faceted," with perhaps six facets of roughly equal size around the perimeter.

At four locations around the Loop (three in the southeast quadrant and one the west) there are well-defined indentations in the X-ray shell. There is a local maximum in the X-ray surface brightness immediately interior to each of these indentations (KKPL). All of the indentations have some optical emission associated with them. The two indentations which are brightest in X-rays are also the most conspicuous optically, and are located on the optically bright east and west limbs. (It could perhaps be argued that the entire northeast facet of the Loop is also such an "indentation," but on a much larger scale.) It is a straightforward conclusion from the observations that, when the internal pressure of a remnant is high enough, encountering more material in a given radial direction will retard radial growth, enhance the X-ray emission, and result in

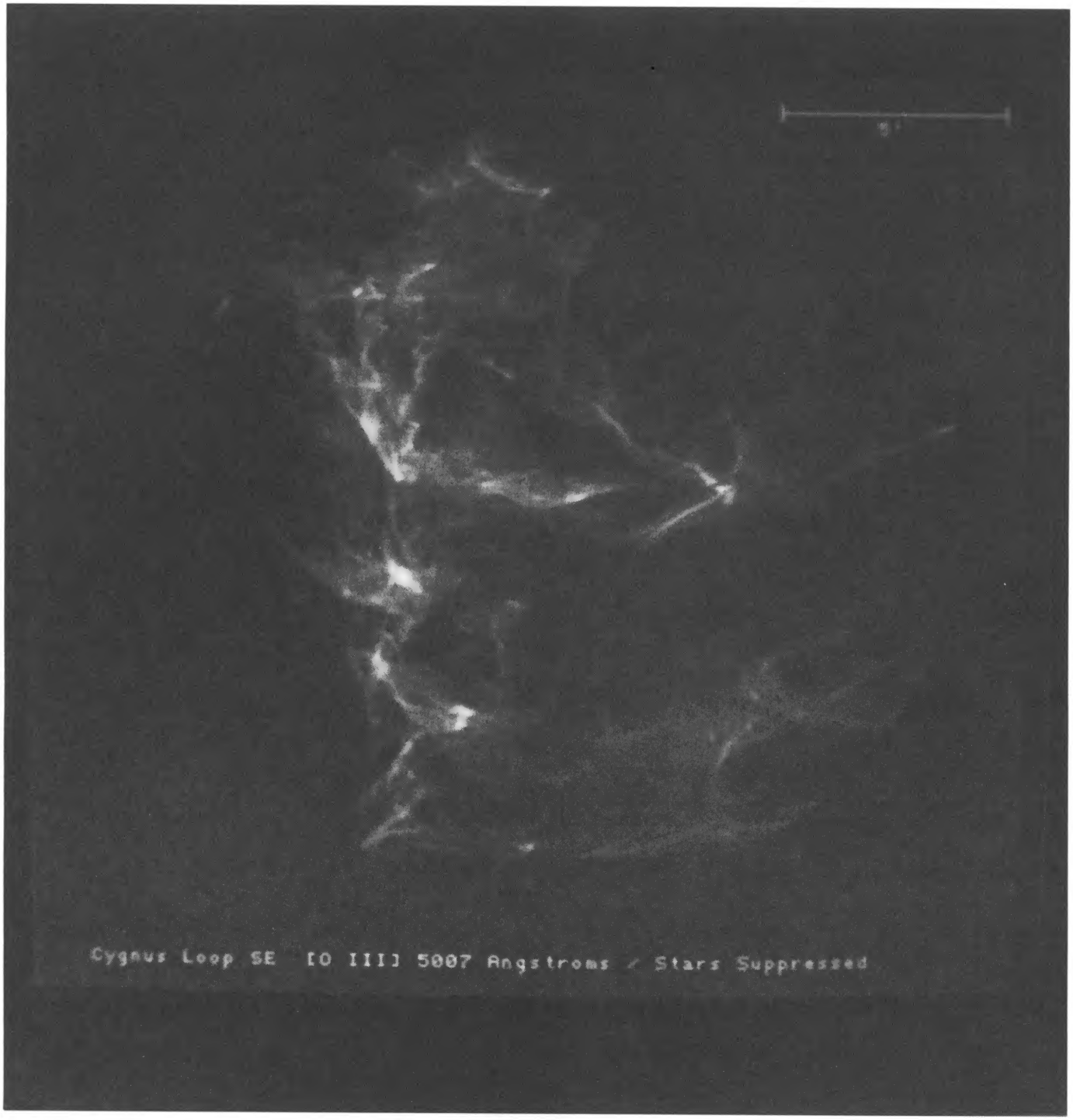

FIG. 2a

FIG. 2.—Linear gray scale maps of the optical emission from the 18′ diameter central region of the field shown in Fig. 1. The maps were generated from image-tube plates taken with the CITD camera on the No. 1, 91 cm telescope at KPNO. They show emission from (*a*) [O III] λ5007 and (*b*) [S II] λ6725. The stars have been suppressed, and the noise has been reduced by 2 σ rejection of pixels over a 3 × 3 pixel window. North is at the top of the figure, and east is to the left. The scale is given by the bar at the top of the figure, which has a length of 5′.

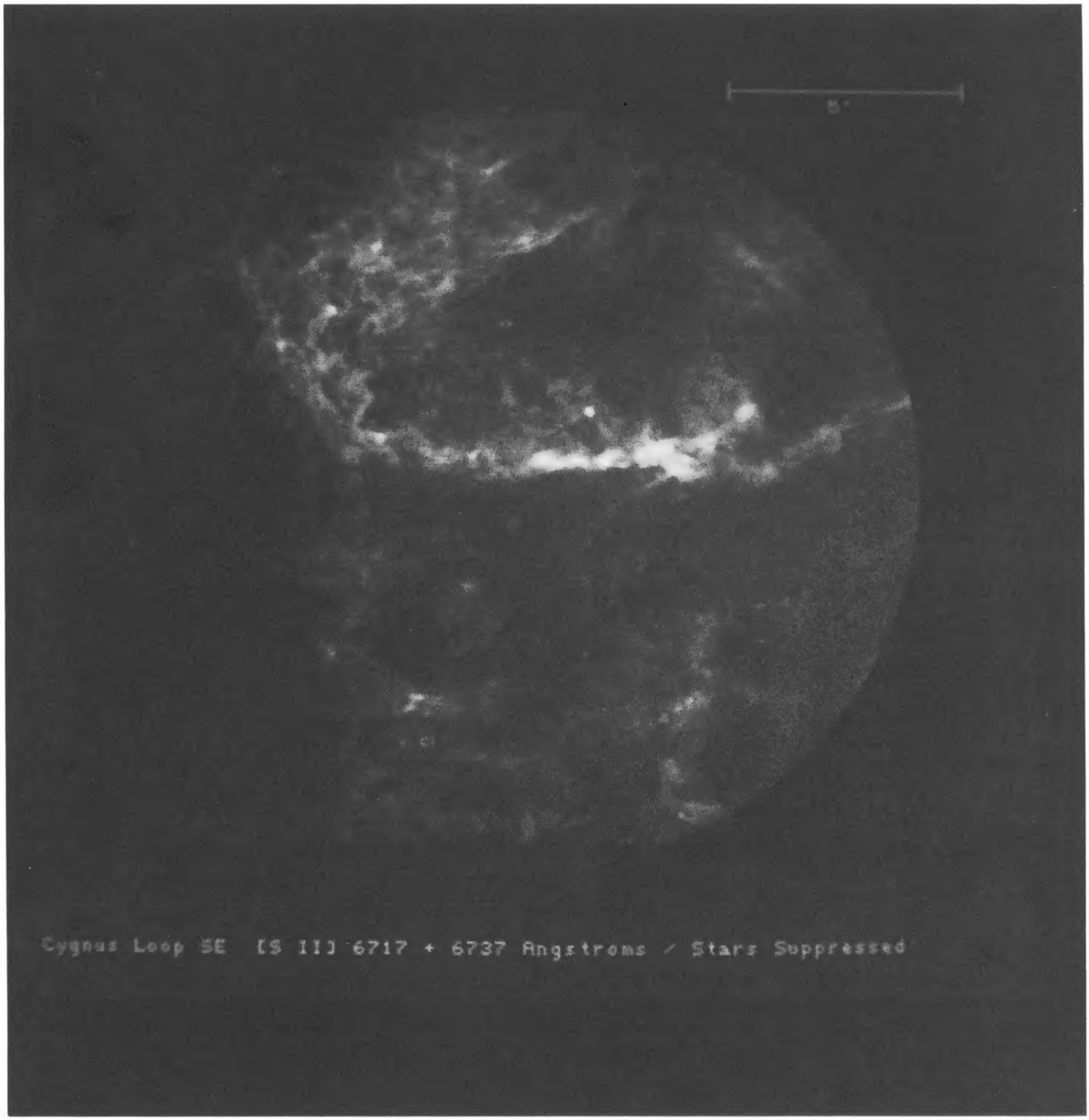

FIG. 2*b*

a greater likelihood of associated optical emission. The relationship between these effects depends sensitively on the densities available, the amount of time since encountering the higher density, and the manner in which mass is distributed between the various phases present.

KKPL go to some effort to establish the reality of exceedingly faint X-ray emission ($\sim$30% of the diffuse background) extending $\sim$10′ beyond the bright shell. This is especially prominent just outside the portions of the shell which are brightest in X-ray emission. If this emission is physically associated with a precursor of the blast wave (consisting perhaps of suprathermal particles or accelerated material which has overrun and now precedes the blast wave), it would be very interesting. A likely explanation for this emission, however, appears to be scattering of emission from the bright shell by grains in the encountered cloud or the intervening ISM, as has been suggested for the X-ray halos around the Crab and Cas A by Mauche and Gorenstein (1984).

There are several regions of higher than average X-ray surface brightness associated with optical emission across the face (i.e., not the limb) of the loop (KKPL). The most notable of these is the region of optical emission in the northwest part of

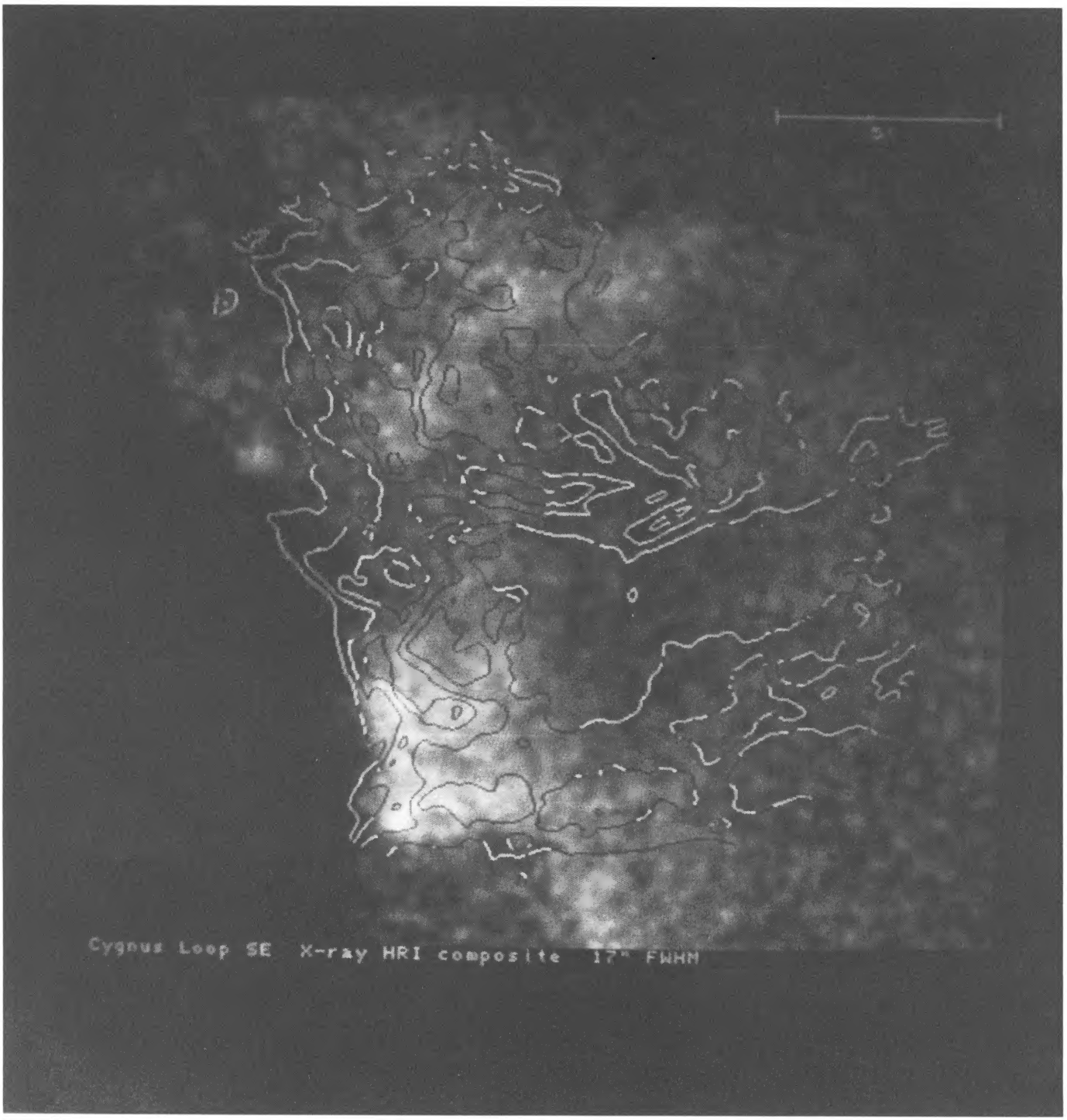

FIG. 3*a*

FIG. 3.—Logarithmic surface brightness contours for (*a*) [O III] and (*b*) [S II] overlaid onto the X-ray map shown in Fig. 2. The optical rasters were smoothed by convolution with a 17″ FWHM Gaussian to match the resolution of the X-ray map before the contours were generated. The contours can be easily interpreted by comparison with Fig. 2. Stars were suppressed before the smoothing so that starlight would not contaminate the nebular contours. The separation between contour levels is a factor of 2.

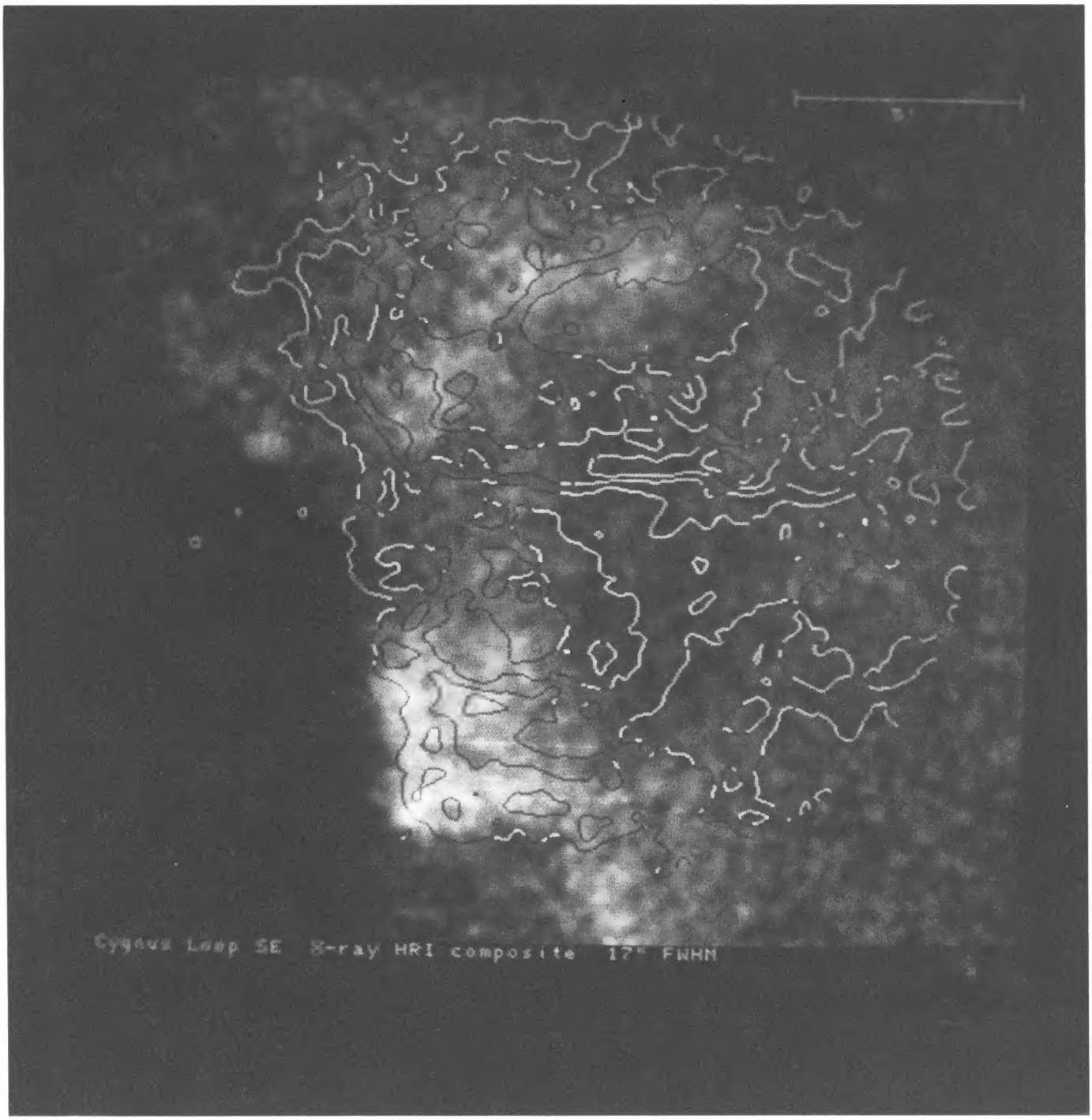

FIG. 3*b*

the Loop ($\alpha = 20^h47^m$, $\delta = 31°20'$). Often referred to as the "carrot." Regions of optical emission along the rim of the Loop could well be carrot-like regions turned more edge-on. If this is so, then the contrast (presumably due to limb brightening) between the moderate X-ray surface brightness at the carrot and the high surface brightness on the rim (a factor of ~ 4) requires that the region of X-ray emission associated with the optical features be fairly thin.

b) Detailed Comparisons for the Southeast

Initially, it seems clear that a general one-to-one relationship between X-ray features and optical features is not to be expected in the Cygnus Loop.[5] The optical emission is thought to arise from very thin ($\leq 10^{16}$ cm) cooling and recombination regions ($T \approx 10^3$–10^5 K) located behind relatively slow shocks (70–120 km s^{-1}) propagating into a medium with a density of order 2–10 cm^{-3}, while the X-ray emission is characteristic of thermal emission from a 2×10^6 K plasma behind an approx-

[5] A detailed one-to-one correlation between optical and X-ray emission may in fact be expected if the scale of the optically emitting clouds is much smaller than the resolution of the images. In this case the warm clouds and the surrounding hot medium would appear to occupy the same volume. This possibility is discussed in § IV.

imately 400 km s^{-1} adiabatic blast wave moving into a medium with density of order 0.1–1 cm^{-3}. On the other hand, the rough correlation which exists between the X-ray and the optical emission on large scales suggests that conditions which lead to optical emission also favor enhanced X-ray emission from the nearby hot medium. On small scales one might hope to find some pattern in the association between optical and X-ray features which would help to clarify the physical relationships and mechanisms involved.

i) *An Escarpment and XA*

Figure 4 shows a schematic drawing of the field in the southeast with a number of features and regions labeled for discussion. A steep escarpment in the X-ray surface brightness runs along the eastern side of the field. Immediately to the left of this line the X-ray surface brightness is ~ 0.01 counts $arcmin^{-2}$ s^{-1}. This surface brightness is comparable to the "unenhanced" limb brightness around much of the Loop, and we refer to this level as the "local shell level." The surface brightness declines to the east of this point down to 0.001 counts $arcmin^{-2}$ s^{-1} (which defines the edge of the X-ray shell in the composite IPC map from KKPL) about 10′ from the escarpment. The contrast across the escarpment varies from a factor of ~ 2 to a factor of 17. The lowest surface brightness in the field to the west of this line is 0.024 counts $arcmin^{-2}$ s^{-1}, which is still a factor of 2 brighter than the emission interior to the Loop about 30′ to the west.

The entire X-ray region XA, located in the southeast part of the field, sits at the nose of one of the previously mentioned indentations in the X-ray shell. Figure 5 shows an enlargement of XA. Figure 5*a* is a linear gray scale map of the smoothed X-ray emission overlaid with X-ray contours. The contours are logarithmic, with each contour separated from its neighbors by a factor of $2^{1/2}$. The lowest contour level is 0.035 counts $arcmin^{-2}$ s^{-1}. Figure 5*b* shows these same contours overlaid on a logarithmic gray scale map of the unsmoothed [O III] emission. A logarithmic gray scale was used so that both the faint and the bright optical structure would be visible. The eastern edge of XA overlaps the field which Teske and Kirshner (1985) imaged in [Fe X] λ6374 coronal line emission. They found that the coronal line emission has a distribution similar to that of the X-ray emission, but with features loosely correlated with the bright optical nebulosity. The average X-ray surface brightness in the region is ~ 0.09 counts $arcmin^{-2}$ s^{-1}. Along the eastern edge of XA the average surface brightness is ~ 0.11 counts $arcmin^{-2}$ s^{-1}, 11 times the local shell level. At the southeast corner of XA there is a small knot with a surface brightness of 0.17 counts $arcmin^{-2}$ s^{-1}, placing it among the brightest X-ray features in the Loop. The knot sits between the branches of a Y formed by two [O III] filaments. Assuming a temperature of 2×10^6 K, a spherical geometry, and a radius of 10″, KKPL calculate a density of 31 cm^{-3} for this position, and suggest that the density may actually be higher if T is lower. This density is 10–100 times the average density behind

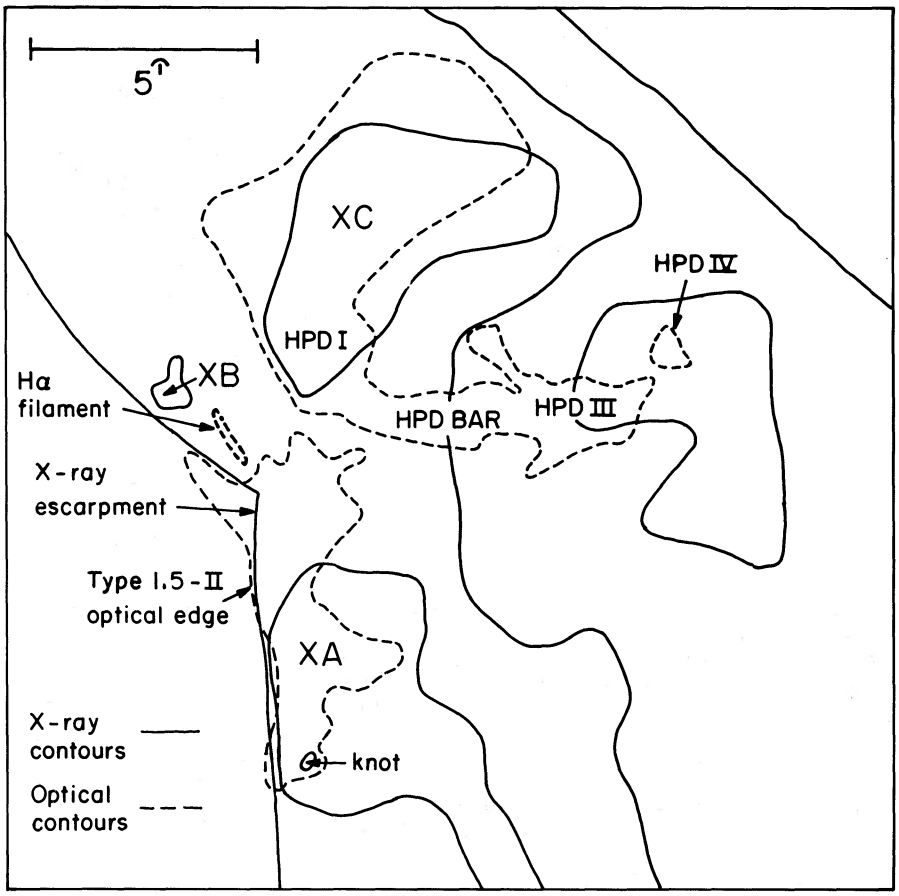

FIG. 4.—Schematic drawing of the field studied, with features and regions labeled for discussion

the adiabatic blast wave (as calculated from Sedov fits to the X-ray data or pressure balance with the optical shocks) and is comparable to the density behind the radiative shocks before cooling.

1. *Optical appearance of XA.*—Optically, the vicinity of XA contains a complex of features which are primarily type I.5 and type II. (Type I.5 and type II are HPD's notation for features which are strong in [O III] but weak or absent in emission from optical lines of cooler species.) The X-ray emission in Figure 5 is roughly divided into northern and southern sections by a somewhat fainter wedge which intrudes from the west. These sections are more or less outlined by the fourth contour level in Figures 5*a* and 5*b* (~ 0.1 counts arcmin^{-2} s^{-1}). The northern section is overlaid on a triangular region of optical emission which includes a closely spaced pair of bright knots, lying about 2′ west of the optical edge. These knots are present in both [O III] and [S II]. In [O III] there are bright flaring filaments to the east of these knots, suggesting a shock wrapping around a dense "nose" or "trunk" on the face of a larger cloud. There is a moderately bright X-ray knot located just to the west of the optical knots, and the X-ray brightness is broadly peaked just east of the flare. Another bright optical knot visible in both [O III] and [S II] is located 2.5 northeast of the former. At this location, the X-ray escarpment is more diffuse and dented inward to the edge of the optical knot, much as in the large-scale structure. The western part of the southern section of XA, on the other hand, fills a void in the optical emission. The western edge of XA, as defined by the third contour level in Figure 5 (0.07 counts arcmin^{-2} s^{-1}), lies 30″–45″ to the west of a faint north-south [O III] filament.

Within XA there is neither a consistent correlation nor an anticorrelation between the optical and the X-ray emission. (There are, in fact, striking examples of each.) The eastern and southern *borders* of XA are another matter. A very striking correlation exists along the eastern edge of XA, where the edge of the bright X-ray emission and the envelope formed by the leading optical filaments are coincident to well within the limits of resolution and alignment of the data. The X-ray escarpment follows the optical edge for a distance of well over a parsec. This sharp edge is also present in [Fe X] λ6374 emission (Teske and Kirshner 1985) and in 49 cm synchrotron emission (Dickel and Willis 1980). At the southern end of XA the X-ray contours above about 0.05 counts arcmin^{-2} s^{-1} make a sharp turn to the west and follow a group of east-west optical filaments for about 4′ (~ 0.9 pc) before turning again to the south. The north-south ridge in the X-ray surface brightness is still pronounced at the southern edge of the field. From the IPC map it appears that this ridge follows the edge of the optical emission $\sim 5'$ to the southwest.

2. *Geometry of XA.*—The relationship between the optical and the X-ray emission at XA is complicated in detail, but on the whole is most easily understood as a thin but distorted sheet of optical emission *interior to which* is found a somewhat thicker slab of bright X-ray emission. The projected thickness of the bright eastern portion of XA ($\sim 1' \approx 0.2$ pc) provides an upper limit on the physical thickness of the region of enhanced X-ray emission there. (The size of the bright knot, $\sim 20''$, gives an estimate of ~ 0.07 pc for the thickness of the region.) This is considerably less than that expected for emission behind the adiabatic blast wave propagating into a uniform preshock medium in a typical Cygnus Loop model.

The geometry of the bright knot in XA may not be spherical. When describing bright optical features, it is often necessary to invoke a line-of-sight depth much greater than the apparent thickness of the feature (Parker 1967; Miller 1974) or the expected thickness of the radiative zone behind a shock (HPD). (Most filaments are about 15 times as bright as a face-on shock, and factors of up to 50–60 occur—face-on 100 km s^{-1} shocks are essentially invisible on our plates.) If the greatest line-of-sight depth in the area is comparable to the north-south elongation of XA (4′ ≈ 0.9 pc—this trick often works fairly well for the optical data), then the emission measure given by KKPL (~ 77 cm^{-6} pc) gives $n \approx 9$ cm^{-3}.

3. *Pressure equilibrium?*—The knot in XA (and probably all of XA) appears to have a considerably higher pressure than is generally inferred for the postshock region. Assuming a constant $N_H = 4 \times 10^{20}$ cm^{-2}, KKPL found that the limb temperature is fairly constant (within a factor of ~ 2) at about 2.1×10^6 K, with a slight anticorrelation between temperature and surface brightness. This anticorrelation is in the right direction for pressure equilibrium. (A similar but more quantitative result has been reported for the Vela SNR by Kahn *et al.* 1984.) Thus, the knot may have a slightly lower than average temperature, but the inferred densities are high. At $T = 6 \times 10^5$ K (considerably lower than any temperature reported by KKPL and probably somewhat too low for strong X-ray production at all), $n = 31$ cm^{-3} and 9 cm^{-3} give $p/k = 38 \times 10^6$ cm^{-3} K and 11×10^6 cm^{-3} K, respectively. This compares with $p/k = 2nT = 2.6 \times 10^6$ cm^{-3} K for the average Sedov parameters and a usual [S II] optical pressure of $p/k < 7 \times 10^6$ cm^{-3} K (assuming $n_e < 10^3$ cm^{-3}, 50% ionization, and $T = 5000$ K).

The relative overpressure of the knot can be demonstrated more clearly by comparing its surface brightness with unenhanced parts of the shell. The line-of-sight depth through the brightest part of a 1 pc thick shell with radius 20 pc is ~ 12 pc. The depth through the brightest part of a shell with radius 20 pc and a limb-to-center ratio of 3:1 is ~ 24 pc. Thus, for a region only 1 pc deep to appear 17 times brighter than the local shell level requires that it be 15–20 times denser. Since the temperature cannot be more than about a factor of 2–3 lower in the bright regions, this requires that the pressure be higher by a factor of at least 5–7.

ii) *XB and XC*

Just north of XA the X-ray surface brightness drops off to ~ 0.06 counts arcmin^{-2} s^{-1}. The optical emission remains strong at this location, especially in [O III]. At this point both the optical and the X-ray edges turn to the northeast, with a relatively modest rise in X-ray emission occurring about 30″ behind an [O III] arc. The X-ray feature XB (which has a peak surface brightness of ~ 0.10 counts arcmin^{-2} s^{-1}) and the X-ray arc extending northeast from there lie just behind the geometrical extension of the [O III] arc. This arc forms the sharp southeastern boundary of the diffuse optical emission to the east of HPD's region I. This diffuse emission is spectrally similar to the arc itself (see the extreme southeast corner of Figs. 4 and 5 in HPD) and also fades out gradually along its northeastern extent. Roughly speaking, the appearance is that of a bubble-shaped surface which grows progressively fainter in optical emission toward its northeastern end, with XB lying just inside the bubble. XB, however, is unique in that it is the only bright spot of X-ray emission that is not directly associated with a local optical feature or irregularity. There is also a

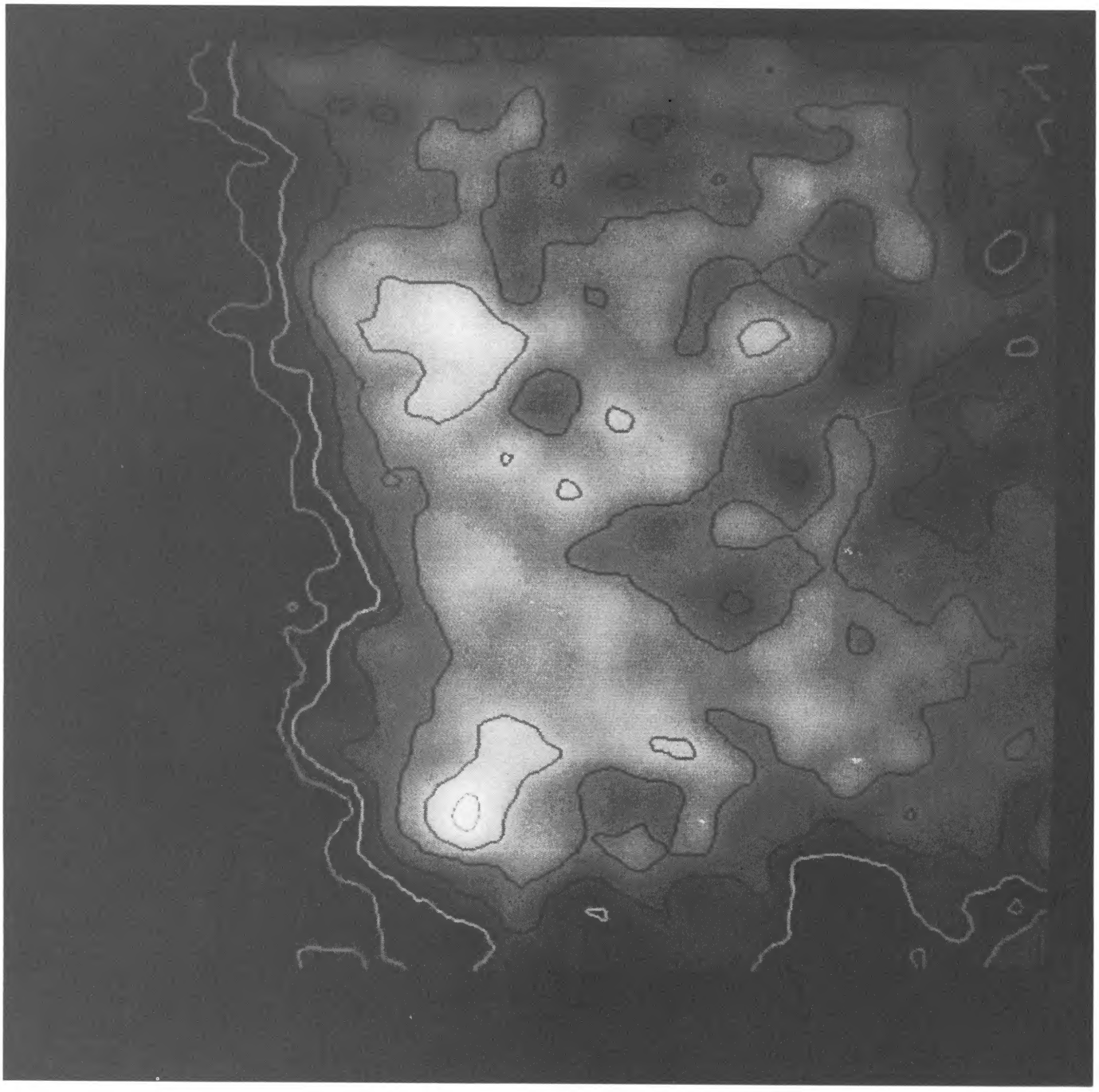

FIG. 5a

FIG. 5.—Enlargement of the X-ray region XA. (*a*) Linear gray scale map of the smoothed X-ray emission, overlaid with logarithmic X-ray contours. The lowest contour level is 0.035 counts arcmin^{-2} s^{-1}, and each contour is separated from its neighbors by a factor of $2^{1/2}$. (*b*) These same contours are shown overlaid onto a logarithmic gray scale map of the unsmoothed [O III] emission. A logarithmic gray scale was used so that both the faint and the bright optical structure would be visible. The most remarkable detailed correlation between the optical and the X-ray emission occurs along the eastern edge of the region.

very faint Hα filament (apparently similar to the "pure" Balmer filaments discussed by Raymond *et al.* 1983 and others) lying near the edge of the X-ray emission between XA and XB.

The bright X-ray region XC has an average surface brightness approximately 8 times the shell level ($\sim$0.08 counts arcmin^{-2} s^{-1}) and is roughly defined by the 0.065 counts arcmin^{-2} s^{-1} contour. It is associated with a region of mottled optical emission (HPD's region I and its continuation to the north). The southeast edge of XC closely follows the edge of the bright [O III] emission in HPD's region I. Less than 1′ west of that edge there is a second X-ray "filament" which lies just interior to a bright optical filament visible in both [O III] and [S II]. (See Figs. 2 and 3.) There are a number of locations across XC where small X-ray features lie on top of or just to the west of optical features. The anvil shape of XC generally matches the extent of the [S II] emission, although the X-ray emission extends slightly farther to the west than does the optical emission. XC could be explained by a flat 0.2 pc thick zone of enhanced X-ray emission (much like XA) turned somewhat face-on. *As is the case with XA, the X-ray emission gener-*

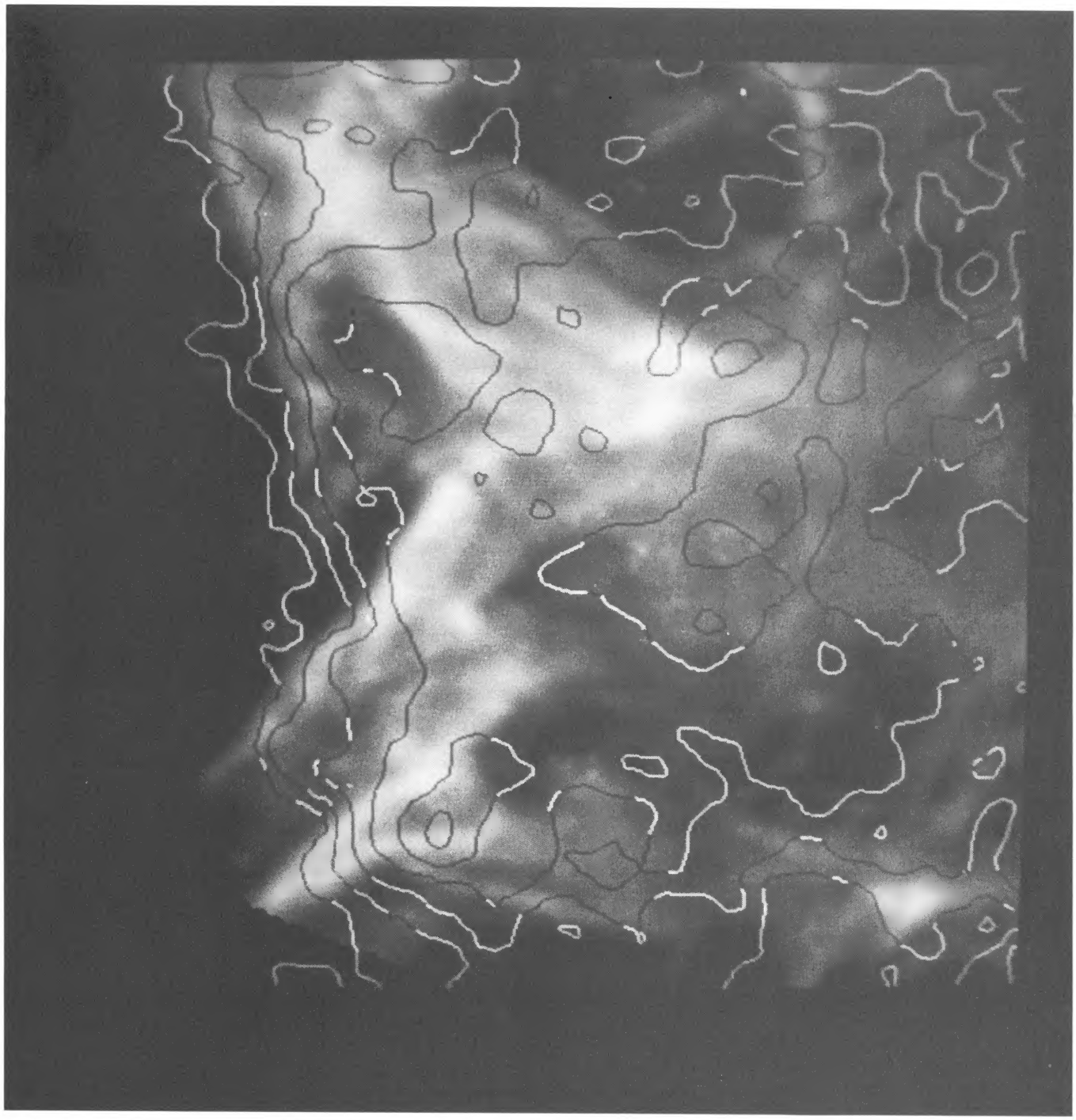

FIG. 5*b*

ally appears to lie physically interior to the optical emission with which it is associated.

There is an irregular region which is very slightly enhanced in X-rays extending to the west of HPD's region III. This region has an average surface brightness of ~ 0.052 counts arcmin^{-2} s^{-1}, as compared with 0.038 counts arcmin^{-2} s^{-1} for the fainter emission between it and XA and 0.024 counts arcmin^{-2} s^{-1} for the faint region in the northwest corner of the field.

There are several regions of strong optical emission which do not show exceptionally bright X-ray emission. The western end of the horizontal bar located just east of region III shows no enhancement at all in X-rays relative to the surrounding emission, although it is particularly bright in [S II]. HPD's region IV, located in the northwestern part of the field and visible only in lines from low-excitation species, is not strongly enhanced in X-rays. There is also some faint optical emission in the southwest corner of the field which is not enhanced in

X-rays. Note, however, that even the "unenhanced" X-ray emission in the western part of the field is still fairly bright by the standards of the Loop as a whole.

c) *Coincidence of Bright Emission with the Blast Wave*

We discussed the striking correlation between an X-ray escarpment and the edge of the optical emission along the border of XA and extending on to the patch of emission 5′ southwest of our field. The coincidence between edges of regions of X-ray and optical emission is also found elsewhere in the Cygnus Loop. The bright X-ray knot on the west limb discussed by KKPL appears to be associated with radiative shocks in much the same way as XA. There is also a close correlation between the edge of the X-ray shell and the optical features along the eastern limb of the breakout in the south. KKPL discuss the correlation of the edge of weak portions of the X-ray shell with optical filaments which are primarily visible in Balmer-line emission from hydrogen (Raymond *et al.* 1980*b*, 1983; Gull, Parker, and Kirshner 1977). On the basis of spectral characteristics and a two-component Hα velocity profile similar to that reported by Treffers (1981), Raymond *et al.* (1983) have suggested that the Hα emission is due to collisional excitation of neutral hydrogen behind a collisionless nonradiative shock with $v \approx 170$ km s^{-1} moving into a medium with $n_0 \approx 2$ cm^{-3}.

An edge in the X-ray emission as sharp as the eastern border of XA is most easily interpreted as a portion of the blast wave which is tangential to the line-of-sight. The coincidence of optical features with well-defined X-ray escarpments or the edge of the X-ray shell suggests that at these locations the locus of optical emission is coincident (within a cooling length of $\sim 10^{16}$ cm) with the current position of the blast wave. This view is strengthened by the young age of the optical emission at XA (see § III*d*). The geometry of XA and its location at the nose of an indentation are consistent with an encounter between the blast wave and a cloud having dimensions of a parsec or greater. This may apply to all of the regions of optical emission, our being prevented from seeing it by the fact that the other regions do not lie as close to the projected edge of the Loop. Cox (1972) suggested that about 12% of the surface of the Loop is covered with radiative shocks. If this estimate is accurate, then it is fortuitous that we see optical emission at the actual projected edge at all.

The view that the blast wave and optical emission are coincident is quite different from that of other authors (e.g., Fesen, Blair, and Kirshner 1982; Teske and Kirshner 1985), who assume that complexes of optical emission seen in projection 5′ interior to the X-ray edge *physically trail* the blast wave by a parsec. The difference between these views is perhaps the central issue in understanding the Cygnus Loop.

The strong X-ray escarpment in our field is well correlated with the leading bright optical filaments. (As discussed above, the same appears to be the case at other locations around the Loop.) Fainter X-ray emission does extend 5′–10′ farther out, however. This tendency for X-ray emission to extend beyond the bright optical filaments (as well as bright X-ray features) is expected from geometrical effects alone. Since the shell is complete in X-rays, X-ray emission is guaranteed to be seen at the projected edge of the shell. Conversely, the patchy and comparatively rare optical emission should normally be seen near *but not at* the projected edge. Assuming a perfectly spherical geometry, about one-third of the surface area of the Loop is seen in projection within 5′ of the edge. At the canonical distance of the Cygnus Loop, a 5′ projected distance from the edge corresponds to a spatial distance of 7 pc measured along the shell surface. The observed separation between X-ray and optical edges at best represents only a strong upper limit on the difference in radii between the optical and X-ray shells. The coincidence of the X-ray escarpment with bright optical filaments in our field (and possibly elsewhere) implies that bright X-ray features do occur in conjunction with optical features and that both are patchy, strongly suggesting that both lie at the local outer boundary of the shell.

It might be argued that, since line-of-sight tangency is absolutely required to achieve the surface brightness of the optical filaments, they must lie at the projected edge. Such is not the case, however. Even small ripples on a smooth sheet will produce line-of-sight tangencies so long as the average sheet normal is close to perpendicular to the line of sight (Hester 1985). (The maximum angular difference for achieving tangency equals the angular perturbations of the ripples.) This effect further enhances the likelihood that the brightest optical features will, in the absence of large-scale deformation of the shell, be generally near the projected edge.

Finally, it must be recalled that our field, and XA in particular, lies at the nose of an indentation into the X-ray shell, even as defined by the weak contours. Similar indentations are accompanied by bright X-ray and optical emission at other locations as well. Emission located at the nose of an indentation will always appear in projection to lie interior to the edge, even if it is physically coincident with the local outer boundary of the shell.

In summary, *there is no compelling evidence that the regions of bright optical emission are all substantially interior to the local outer boundary of the shell* (*i.e., the local position of the blast wave*), *and in fact it seems almost certain that many are not.*

d) *Recency*

In the notation of HPD, the optical emission associated with the bright X-ray region XA, and in particular the emission coincident with the edge of XA, is type I.5 to type II. HPD follow others (Raymond *et al.* 1980*a*; Fesen, Blair, and Kirshner 1982) in interpreting type II emission as due to emission from young incomplete cooling regions. This implies a recent encounter between the blast wave and the cloud, since the degree of completeness of the cooling region is directly related to the amount of time since the material behind the shock first began to radiate. This interpretation is strengthened by the fact that feature type correlates with the spatial order of features in the way expected (HPD), with incomplete cooling regions generally found ahead of complete cooling regions. The transition from a nonradiative shock to a radiative shock approaching steady flow can be seen along the length of the [O III] arc between XA and XB. At its western end, this arc is visible in relatively cool lines such as Hα and [S II], as well as [O III]. Moving to the east and north, the arc disappears in all lines but [O III], then fades out in the optical entirely, only to appear again in X-rays about 30″ farther along. (We predict that UV and possibly [Fe X] observations of the gap would show the presence of a shock with $v > 130$ km s^{-1}.) *This appears to be the location where the blast wave is attached to the cloud or portion of a cloud responsible for the optical emission at XA.*

In contrast to XA, HPD's region III (the vicinity of position 2 of Miller 1974) seems a very good candidate for a cloud which has in fact been largely or wholly engulfed by the blast

wave. It is the site of very bright optical emission from lines ranging in ionization state from O^{++} through S^{+} and O^{0}, which implies that the blast wave hit the cloud (or passed through the region) much longer than a cooling time ago. The geometry of region III and the filaments which emanate from it to the northeast and southeast further suggest that it is a significant indentation into the shell. The projected distance of region III behind the edge of the bright optical emission is slightly over a parsec. Despite its evolved state, this region is not at all conspicuous in the X-ray image. It appears, then, at least for the field studied, that exceptionally bright X-ray emission must be viewed as a phenomenon associated with a recent encounter with the blast wave, rather than as a phenomenon associated with prolonged exposure to the hot medium behind the blast wave.

e) Synopsis

A physical description of the Cygnus Loop must accommodate the following facts.

At X-ray wavelengths, the Cygnus Loop is a limb-brightened shell with a thickness of $\gtrsim 1$ pc and a limb-to-center ratio of roughly 3:1 to 5:1. There are extended pancakes of X-ray emission (which are about a factor of 2 brighter than the unenhanced shell) surrounding regions of exceptionally bright X-ray and optical emission. The brightest X-ray emission lies at noses of indentations into the shell. Optical features at several locations are coincident (at least down to scales that can be judged from the IPC map) with edges or ridges in the X-ray emission.

On smaller scales there are regions of X-ray emission (e.g., XA and XC) which are ~ 10 times as bright as the unenhanced shell. These regions sometimes agree in general extent with regions of optical emission, although regions of optical or X-ray emission exist without counterparts in the other band. In particular, an evolved region of optical emission located ~ 1 pc west of the projected bright optical edge is not particularly bright in X-rays. When optical and X-ray emission do go together, the X-ray emission appears to lie physically just interior to the optical emission. (We find no compelling evidence to support the claim that optical filaments lie substantially interior to the local position of the blast wave.) Within the bright X-ray regions are smaller features which are a factor of ~ 2 brighter still. The regions of brightest X-ray emission seem to be significantly out of pressure equilibrium with the rest of the shell's interior.

At the scale of our resolution there is no general one-to-one correlation between X-ray and optical emission. A significant exception to this occurs along a sharp escarpment in the X-ray surface brightness across which the surface brightness jumps by a factor of 2–17. The escarpment is coincident with young ($\lesssim 10^3$ year old) optical emission over a length of more than 1 pc.

IV. DISCUSSION

The gross correlation between optical and X-ray emission has led some authors to suggest that the clouds responsible for the optical emission may be evaporating and that the evaporated material is enhancing the X-ray emissivity (e.g., Cowie, McKee, and Ostriker 1981; KKPL) and coronal line emissivity (e.g., Ballet, Arnaud, and Rothenflug 1984; Teske and Kirshner 1985) of the intercloud medium. We will discuss evaporation and attempt to evaluate its effect on X-ray emission quantitatively. We will also consider three alternative means of achieving brighter than average X-ray emission based on conditions which will almost certainly be present and which may be more important than evaporation. These are (1) a preexisting higher density of the preshock intercloud medium in the vicinity of the clouds responsible for the optical emission; (2) an increase in the pressure behind the blast wave caused by rapid deceleration as it runs up a density gradient; and (3) further compression and heating of the hot postblast flow by reflected or bow shocks associated with dense clouds.

a) Two Pictures of the Cygnus Loop

Before discussing evaporation, we will outline the overall physical picture it presupposes. Briefly, the blast wave enters a region containing many clouds or cloudlets and propagates more or less unimpeded through the intercloud medium. Radiative shocks are driven into the clouds, giving rise to the optical emission. The clouds are engulfed by the hot flow behind the blast wave and partially or completely evaporate, enhancing the density of the X-ray emitting intercloud component. Since for a range of temperatures the X-ray volume emissivity of the intercloud medium increases faster with density than it decreases with temperature, the evaporated material has the net effect of enhancing and softening the X-ray emission.

Variations of this picture, coupled with the notion of thermally unstable cloud collapse and/or extremely small cloudlets, have been used by a number of authors to explain the filamentary structure of SNRs such as the Loop (e.g., McKee and Cowie 1975; Dickel and Willis 1980; Smith and Dickel 1983), the correlation of optical and radio emission (Straka *et al.* 1983), optical and UV spectra which suggest the existence of nonsteady flow shocks (Raymond *et al.* 1980*a*; Fesen, Blair, and Kirshner 1982), and the variations in the appearance of the Loop when viewed in the light of different emission lines (Fesen, Blair, and Kirshner 1982).

We find it somewhat difficult to compare our observations with this picture because it does not really represent a single viewpoint. No proponent has ever tried to present it in a consistent form, taking into consideration all of the relevant observations. The question of cloud sizes is central to this difficulty. The standard model of an evaporative SNR is that of Cowie, McKee, and Ostriker (1981), who use cloud radii of order 2 pc and integration step sizes which smooth over the structure on the scale of our observations. Fesen, Blair, and Kirshner (1982) use cloud sizes which are $\ll 0.01$ pc and view the optical filaments essentially as ensembles of these tiny cloudlets. KKPL and Teske and Kirshner (1985) discuss clouds with sizes between 0.06 and 0.12 pc in order to account for fluctuations in the X-ray and [Fe X] surface brightness. An additional difficulty is that the dynamical effects of the clouds on the propagation of the blast wave itself have not been adequately discussed. If the cloud filling factor is large (which it must be if evaporation is to affect the intercloud medium as dramatically as the data seem to suggest and if the optical surface brightness is to be achieved), then the assumption that the blast wave propagates freely through the intercloud medium may not be valid. Even without considering the evaporated material, the drag and/or "shadows" of clouds could significantly affect the flow behind the blast wave. (The situation may be analogous to forcing a fluid through a porous plug.) A model of the propagation of the blast wave through a cloudy medium which (1) kept track of the dynamical effects of clouds and the material evapo-

rated from them and (2) followed the fate of the optical, X-ray, and coronal line emission would be very useful. It is our feeling that such a model would have difficulty in simultaneously accounting for all of the phenomena that this picture has been invoked to explain.

A different physical picture has also been used to explain the filamentary and spectral structure of the Loop (HPD; Hester 1985). If the clouds responsible for the optical emission are as large as filament lengths or larger (perhaps resembling "standard" interstellar clouds [Spitzer 1978], or even outer portions of molecular clouds), and if thermal instabilities are relatively ineffective in fragmenting the cooling region (as is suggested by the ubiquitous presence of small-scale features emitting in a wide range of emission lines), then the source of the optical emission would more closely resemble a thin ($\sim 10^{16}$ cm) sheet working its way into the cloud. In this view the projected linear extents of the regions of optical emission around the Loop may be characteristic of the cloud sizes. In other words, the entire east, northeast, and west optical limbs could each represent a single large cloud. (It is well known, but often overlooked, that just such a cloud is probably needed to explain the contrast in star counts on the blue POSS print across a line which coincides with the edge of the optically bright west limb.) DeNoyer (1975) found that there are H I clouds adjacent to the optical nebulosity in the west and northeast. Assuming a line-of-sight depth of 5–10 pc, she calculated densities of 5–10 cm^{-3}. The agreement of the average H I density with the cloud density inferred from the optical data requires a cloud filling factor close to unity, and can be most easily explained by single clouds 5–10 pc in extent. The distribution of such clouds around the perimeter of the Loop could perhaps have been influenced by the supernova precursor (e.g., McCray and Snow 1979; Shull *et al.* 1984).

Hester (1985) demonstrates that variations in projected line-of-sight depth along the sort of deformed thin sheet required in this second picture result in a filamentary morphology remarkably similar to that of the Cygnus Loop. (Such a geometry for the filaments was first proposed by Poveda and Woltjer 1968.) This picture accounts for the observation (HPD) that the optical filaments in the Loop are generally not spectrally distinct from the diffuse emission in which they lie and the fact that the depth of the filaments must be many times their apparent width. Filaments are also often seen to bound regions of diffuse optical emission (e.g., the [O III] arc between XA and XC and the forklike filaments north of center), which strongly suggests limb brightening in a thin sheet. In this picture, variations in the appearance of the Loop when viewed in different emission lines arise from systematic variations in the physical conditions (e.g., shock velocity and completeness of the cooling region) along the face of the sheet. The coronal line emission would arise predominantly in shocked intermediate density material.

The observed correlation of radio and optical features is explained in the standard way using field compression along with "betatron" acceleration of cosmic rays (van der Laan 1962*a*, *b*). Straka *et al.* (1983) noted an apparent trunction of the radio behind [S II] and suggested that it could be explained by a rarefaction wave (Straka 1984). Other possibilities for such a truncation include the limited lifetime of accelerated cosmic-ray particles against escape from the regions of compressed fields, lower compression and acceleration in the slower shocks responsible for the low-excitation filaments, or a sufficiently recent encounter that there simply is not any dense material behind the [S II] zone. Any of these explanations could probably be applied to either view of the cloud scale.

b) Small Cloudlets?

The preceding section makes it clear that a crucial parameter in explaining not only our data but all of the data on the limb of Cygnus Loop is the characteristic size of a cloud in the preshock medium. Judging from the optical and X-ray appearance of the Cygnus Loop, inhomogeneities obviously exist in the surrounding ISM on scales ranging from <0.1 to >10 pc. It is not clear, however, when to call such inhomogeneities "clouds." For the purposes of the current discussion a "cloud" can be thought of as a contiguous region in which the ambient density is high enough for the formation of a radiative shock at the applicable pressure. While this definition is very pragmatic and far from universal, it is obviously useful when one is discussing the optical morphology. It is also appropriate in discussing the X-ray emission, because it takes a "nonradiative" shock to heat the "intercloud" medium to temperatures which can emit X-rays and/or drive significant evaporation. Finally, this definition is appropriate from a dynamical standpoint because it is the material behind radiative shocks which cools and is compressed, leading to very dense regions behind the blast wave.

HPD argues that the optical morphology and spectral structure of the Cygnus Loop require clouds which are large enough for the formation of steady flow shocks and certainly no smaller than the lengths of filaments. Hester (1985) further shows that complexes of short filaments can arise from a single shock front moving into a large cloud. An alternative view of the Cygnus Loop (Cowie and McKee 1975; Fesen, Blair, and Kirshner 1982) holds that the clouds are exceedingly small ($\ll 0.01$ pc) and that optical features are really ensembles of these unresolved cloudlets. Clouds which are smaller than a filament length but larger than 0.01 pc are excluded by the optical data because such clouds could be easily resolved. While structure at this scale is in fact observed, the coherence of filaments on larger scales indicates that such structure is due to irregularities in larger clouds rather than to isolated clouds surrounded by a medium which is an order of magnitude or more less dense.

The evidence favoring large clouds is outlined above. An attempt to explain the optical morphology with the small ($\ll 0.01$ pc) cloudlet picture leads to a number of implausible statements about the ISM. (1) Small cloudlets were invoked to explain filaments which were not seen in all emission lines, and the separations between such filaments. To explain the presence of features which *are* seen in a range of lines, however, requires that cloudlets of a wide range of densities be present. This is necessary so that different cloudlets will have cooled to the point of emitting different lines in the same amount of time. (This also rules out large but very thin sheetlike clouds such as those proposed by McKee and Cowie 1975. It does not rule out sheetlike clouds which are thick enough for the formation of complete cooling and recombination regions behind radiative shocks.) (2) A spatially homogeneous distribution of cloudlets would result in emission which is smeared out behind the blast wave, rather than the filamentary structure observed. Thus filaments must reflect the structure of preexisting agglomerations of cloudlets in the ISM in front of the blast wave. (3) The sharpness of filaments requires that the preexisting agglomerations have very abrupt edges. (4) If the filaments have been engulfed by the blast wave, the preexisting agglom-

erations must be very thin. (5) The optical brightness of filaments requires exceedingly large cloudlet filling factors within the preexisting agglomerations of cloudlets. (6) The agglomerations must be sheetlike rather than filamentary to account for the large line-of-sight depth through the emitting region. (7) In the small cloudlet picture, optical spectra will reflect primarily the underlying spectrum of cloudlet densities. For filaments to be spectrally indistinguishable from the surrounding diffuse emission (HPD) the spectrum of cloudlet densities must be the same in and between agglomerations. (8) To account for the agreement in spectral properties of filaments from all around the remnant (HPD), the spectrum of cloudlet densities must be fairly constant everywhere. In short, while the small cloudlet picture was an interesting idea, it leads to consequences for the ISM which are highly implausible.

c) *Evaporation of Clouds*

The "standard" explanation of the large-scale association between X-ray and optical emission in SNRs such as the Cygnus Loop is evaporative enhancement of the intercloud medium. We will try to evaluate the effect on the X-ray emission both for an isolated cloud or cloudlet and for a general enhancement of the intercloud medium by material evaporated from many small cloudlets.

i) *Evaporation of Isolated Clouds*

Evolution of the X-ray emission from the evaporatively enhanced medium around an isolated cloud is an important calculation for two reasons. First, this is the mechanism suggested by KKPL to account for the bright knot at the corner of XA. Teske and Kirshner (1985) also attribute the clumpiness of the [Fe x] data to evaporation from many small cloudlets. Second, this approximates the early phase of the general enhancement of the intercloud medium by evaporation from many cloudlets.

A number of models of thermal X-ray emission from a hot plasma have been constructed (e.g., Tucker and Koren 1971; Kato 1976; Raymond and Smith 1977). These models indicate that at temperatures around 2×10^6 K line emission dominates the X-ray spectrum. To obtain an X-ray emissivity we summed the line emission from Raymond and Smith (1977) models over an energy range from 0.1 to 4 keV (to approximate the response of the HRI). The model temperatures ranged from 1.6×10^5 to 4×10^6 K. These emissivities were adjusted slightly to account for contributions from continuum emission using values read from Figure 2 in Raymond and Smith. We then assumed pressure equilibrium between the evaporatively enhanced region and the surrounding material and scaled the emissivities by T^{-2} ($\propto n^2$) to obtain relative volume emissivities as a function of temperature (or density). This function peaks around 6×10^5 K, where the volume emissivity is up by a factor of about 4 with respect to emission at 2×10^6 K. Overall, the temperature dependence of the X-ray emissivity in this domain is fairly flat, and it is the variation in n^2 which dominates the volume emissivity.

The standard model of evaporation is that of Cowie and McKee (1977), who calculate the steady state evaporation from a spherically symmetric cloud sitting in a hot medium of temperature T_f far from the cloud. If the evaporative flow from a cloud is subsonic and unsaturated, then it is approximately isobaric. Cowie and McKee (1977) showed that this holds for values of the global saturation parameter $\sigma_0 < 1$. This seems to hold for plausible values of the postshock intercloud density n_1, T_f, and cloud radius R_c for the Cygnus Loop (although the heat flow into extremely small cloudlets may be saturated). Draine and Giuliani (1984) found that for $\sigma_0 = 1$ (the smallest value of σ_0 for which they plotted pressure) the pressure at the cloud surface is only $\sim 5\%$ higher than the pressure far from the cloud.

Note that if $\sigma_0 > 1$, then the $\dot{m}$ used below is too large. We have also neglected the greater interstellar absorption at lower energies which will make lower temperature emission appear fainter. Thus the present effort may overestimate evaporation and its effect on the observed X-ray emission. Given the association of bright X-ray emission with young optical emission, the most severe approximation we have made is probably that the evaporative flow has reached steady state. Time-dependent calculations of evaporation in this early phase would be useful.

We convolved the evaporative temperature profile from Cowie and McKee (1977) (assuming $\phi = 1$, corresponding to evaporation uninhibited by magnetic fields) with the isobaric volume emissivity described above and integrated outward to obtain the average effect of evaporation on the total X-ray emission internal to a given radius. We began the integration at the cloud center to account for the fact that the cloud is a "hole" in the X-ray emission. Figure 6 shows plots of the total X-ray emission for T_{6f} ($= T_f/10^6$ K) = 1, 2, and 4. The results are normalized to the emission from the same volume in the absence of the cloud or the evaporated material. For $T_{6f} = 2$ the volume emissivity peaks within 10% of a cloud radius from the surface of the cloud. The emission from this thin shell is ~ 3 times greater than the unenhanced case. For $T_{6f} = 4$ the peak enhancement in the emission from a thin shell bounded by the cloud surface (a factor of ~ 11.5) comes within $1.01R_c$. The filling factor for this shell is small, however. The net increase in X-ray emission over the volume interior to $1.5R_c$ is only a factor of 1.7 and 2.7 for $T_{6f} = 2$ and $T_{6f} = 4$, respectively. The calculated enhancements do not seem adequate to account for the observed total brightness of the knot in XA (a factor of 17 over the "local shell level") or even the fainter region XB. This is especially true because the line-of-sight depth through the enhanced region around the cloud is likely much smaller than the depth through the surrounding unenhanced medium. (It could, however, conceivably account for the factor of 2 enhancement of XA over the brightness of its immediate surroundings.)

It is tempting to increase the temperature T_f to a large value, thereby increasing the overall X-ray emission from the evaporated material, and then say that the observed temperature of 2×10^6 K comes from this denser, cooler medium. To evaluate this possibility, we calculated an average value for the temperature of the evaporative flow defined by

$$\langle T \rangle \equiv \frac{\int_{R_c}^{R} TL(T)n^2(T, T_f)dV}{\int_{R_c}^{R} L(T)n^2(T, T_f)dV} .$$

Table 1 gives the results of this calculation for various parameters. Generally we find $\langle T \rangle \geq \frac{2}{3}T_f$. The observed temperature 2×10^6 K is not consistent with a value of T_f much higher than (3–4) $\times 10^6$ K. We will also discuss below why the initial intercloud temperature should not be much higher than the temperature after evaporation.

If the evaporating cloud is large, then regions such as XA and XB could be the evaporatively enhanced zones close to the surfaces of individual clouds. This picture better fits the observed geometry of XA, and a (time-dependent) calculation

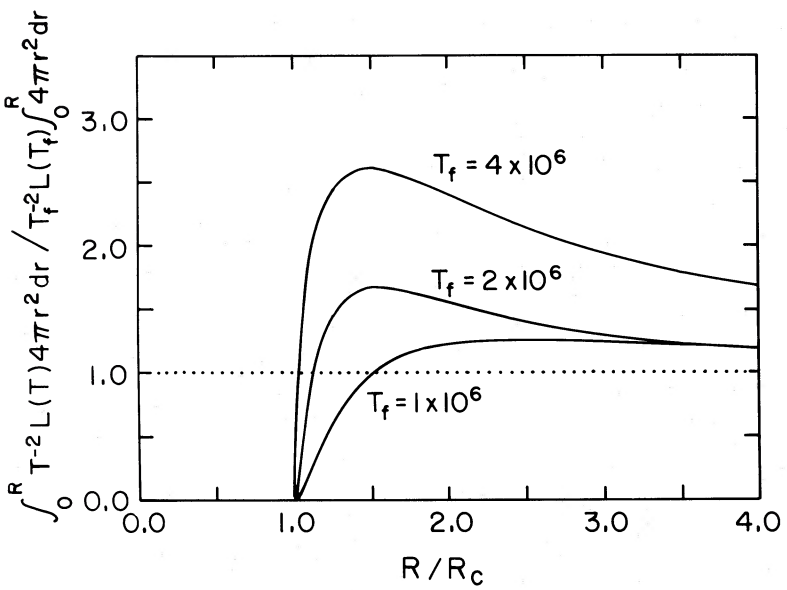

FIG. 6.—Plots of the total X-ray emission internal to a given radius around an evaporating cloud, normalized to the emission expected from the same volume of intercloud medium in the absence of evaporation. The plots take into consideration the fact that the cloud is a "hole" in the X-ray emission. $L(T)$ is X-ray emissivity (ergs cm^3 s^{-1}) calculated from models by Raymond and Smith (1977). The evaporative profile was taken from Cowie and McKee (1977). Pressure equilibrium was assumed.

of the early stages of evaporation from a plane surface would be helpful in evaluating this possibility. It is likely that evaporation will be less efficient in this case. Evaporation off the face of a large cloud would have to occur across the aligned and compressed magnetic field associated with the radiative cloud shock, and will be further hampered by the opposing flow of surrounding material toward the cloud surface.

ii) *General Enhancement of the Intercloud Medium*

If one persists in believing in an abundance of small cloudlets, then the best hope for significant evaporative enhancement of X-ray emission is in using it to enhance the density of the intercloud medium as a whole. This approach was used by Ballet, Arnaud, and Rothenflug (1984), who fitted the [Fe x] and [Fe XIV] coronal line data of Woodgate, Kirshner, and Balon (1977) and Lucke *et al.* (1980) with an evaporative model. They found that the data required a large cloudlet filling factor ($\sim\frac{1}{3}$) and expressed concern that the evaporation may be self-quenching.

1. *Effect of evaporation on the propagation of the blast wave.*—The blast wave is often considered to propagate freely through the intercloud medium. However, if the evaporated material is to become a significant fraction of the intercloud medium (the observations seem to require that it *dominate* the intercloud medium), then there must be a pressure gradient across the evaporation region in order to accelerate the newly evaporated material (Cox 1979; Cowie, McKee, and Ostriker 1981). Assuming that evaporated material is accelerated to $3v_s/4$ at the time of evaporation, the standard equations of continuity of mass, momentum, and energy can be used to relate the flow at a point E in the evaporation region to the flow in front of the blast wave. Let $\langle\rho_0\rangle$ denote the average *preshock* density of the material which has wound up in the intercloud medium at point E. (For example, $\langle\rho_0\rangle = \rho_{IC,0}$, the ambient density of the intercloud phase, if E is taken to be just behind the blast wave where no evaporation has taken place, and $\langle\rho_0\rangle$ equals the average total preshock density for a point E where evaporation is complete.) The solution is

$$\frac{\rho_E}{\langle\rho_0\rangle} = 4\,, \quad p_E = \frac{3}{4}\langle\rho_0\rangle v_s^2\,.$$

The intercloud pressure just behind the shock itself (where conditions in the intercloud medium behind the shock are denoted by the subscript 1) is

$$p_1 = \tfrac{3}{4}\rho_{IC,0}\, v_s^2$$

so

$$\frac{p_1}{p_E} = \frac{\rho_{IC,0}}{\langle\rho_0\rangle}$$

and $T_E = T_1$. In short, for poor dynamical coupling between the clouds and the intercloud component, the temperature in the flow is constant, while the density and pressure rise proportionally.

If the evaporated material dominates the intercloud medium well behind the shock, then $p_1 \ll p_E$. The pressure immediately behind the blast wave, driving it through the unenhanced intercloud medium, will be much lower than the pressure inside the shell. Furthermore, the evaporation zone is approximately isothermal, and the characteristic temperature of the X-ray emis-

TABLE 1

AVERAGE TEMPERATURE[a] OF AN EVAPORATIVE FLOW

	T_{6f}			
R	1	2	4	8
$2R_c$.....	0.65	1.2	2.4	4.4
$3R_c$.....	0.77	1.5	2.9	6.6
$4R_c$.....	0.83	1.6	3.2	6.9

[a] $\langle T_6\rangle \equiv [\int_{R_c}^{R} (T/10^6\ \mathrm{K}) L(T) n^2(T, T_f) dV] / [\int_{R_c}^{R} L(T) n^2(T, T_f) dV]$.

sion is related to the actual blast wave velocity in the same way as in the homogeneous case (i.e., an observed temperature of 2.4×10^6 K implies $v_s \approx 400$ km s^{-1}).

2. *Scale for evaporation.*—The rate at which mass is evaporated off clouds determines the density and pressure gradients behind the blast wave. The rate of change of the intercloud density is

$$\dot{\rho}_{\rm IC} = \frac{N_c \dot{m}}{(1-f)} ,$$

where N_c is the number density of clouds, $\dot{m}$ is the mass loss rate from a single cloud, and f is the cloud filling factor. For the case of unsaturated evaporation, uninhibited by magnetic fields, Cowie and McKee (1977) find

$$\dot{m} \approx 2.75 \times 10^4 T_f^{5/2} R_c({\rm pc}) \ {\rm g \ s^{-1}} ,$$

where the Coulomb logarithm has been set to 30. Integrating the equation for $\dot{\rho}_{\rm IC}$, substituting for $N_c = (3/4\pi R_c^3) f$, and dividing by the average atomic mass yields

$$n_{\rm IC} = 4 n_{\rm IC,0} + 3.30 \times 10^{-6} \frac{f}{1-f} \frac{T_{6f}^{5/2}}{R_c^2({\rm pc})} t({\rm yr}) \ {\rm cm^{-3}} ,$$

where t is the time since the passage of the blast wave. The X-ray emission will increase roughly quadratically with time and distance behind the blast wave until the clouds have been completely evaporated. The time during which clouds will evaporate completely is given by Cowie and McKee (1977):

$$t_{\rm evap} \approx \frac{m}{\dot{m}} \approx 3.3 \times 10^5 n_c R_c^2({\rm pc}) T_{6f}^{-5/2} \ {\rm yr} .$$

To account for the correlation between the optical and X-ray emission along the eastern edge of XA, we will compare the time needed to evaporatively enhance $n_{\rm IC}$ with the time required for clouds to cool enough for the production of optical emission. We will take $n_{\rm IC,0} = 0.16$ cm^{-3} from the Sedov fits and ask how long it takes to enhance $n_{\rm IC}$ by a factor of 4. (This is about what is needed to explain the contrast across the X-ray escarpment along XA.) We will also take $f = \frac{1}{2}$, which is close to optimal for evaporation given the roughly $(1-f)f^2$ dependence (for small f) of the emission measure of the intercloud material. This may significantly overestimate the X-ray emission. The filling factor of clouds engulfed by the blast wave will decrease as the clouds cool. This robs the intercloud medium of thermal energy, reduces the evaporative mass loss by decreasing R_c, and increases the volume to be filled by the hot material. We will neglect these adverse complications.

First we will evaluate the small cloud picture. Taking $n_{\rm IC,0} = 0.16$ cm^{-3}, $T_{6f} = 2$, $n_c = 10$ cm^{-3}, and $R_c = 0.01$ pc results in a time ~ 10 years for a factor of 4 increase in the intercloud density behind the blast wave and a time ~ 60 years for complete evaporation. These times compare with $\sim 700/n_c = 70$ years for the clouds to cool enough to be seen in [O III] and $\sim 2000/n_c = 200$ years for [S II] emission to appear (Raymond *et al.* 1980*a*). The rise in the general X-ray emission occurs almost immediately behind the shock wave (not 1 pc, as supposed by some authors), and the clouds are likely to evaporate completely before cooling sufficiently to emit optical radiation. There is very little observational difference between this case and the case with no clouds and a denser homogeneous preshock medium.

If the cloud radii are taken to be 0.1 pc (this is about the size suggested by Teske and Kirshner 1985), then the time scale for a factor of 4 increase in density is 1000 years, and the clouds do not evaporate completely for 6000 years. In 1000 years a 400 km s^{-1} blast wave will travel 0.4 pc ($\sim 2'$ at $d = 770$ pc). This is consistent with the view that the bright X-ray emission at XA is well behind the blast wave (marked by the projected lower brightness edge). The rise in the X-ray emission from the projected outermost edge of the shell to XA occurs abruptly at the escarpment rather than quadratically, however. This view also does not explain the close agreement in position between the X-ray and optical edges. The rise of the optical emission should still trail the blast wave by less than 10″, putting it close behind the outermost X-ray contour rather than on the X-ray peak. This mechanism could, however, potentially contribute to the X-ray bright spot at the western end of the trunk in XA.

To account for the close correlation between the X-ray and optical emission at XA, we can require cloud parameters such that there is a factor of 4 enhancement of the intercloud density in a cooling time behind the radiative shock. For $T_{6f} = 2$, a radius of $R_c = 0.024$ pc will give X-ray and [O III] emission together at a distance of about 0.03 pc ($\sim 8''$) behind the blast wave. The time for complete evaporation of cloudlets is $t_{\rm evap} = 340$ years, corresponding to a distance of 0.13 pc ($\sim 36''$). This is not too different from what is observed, but does not change the fact that 0.02 pc cloudlets are inconsistent with the optical morphology. We are also uncomfortable with the degree of fine tuning required.

If the correlation of the optical and X-ray emission were due to evaporation from the preexisting agglomerations of cloudlets required by the small cloudlet picture, then a detailed small-scale correlation between the X-ray and the optical emission should exist everywhere, and not just at the leading edge of XA. This is not observed.

If the clouds in the preshock medium are much larger than the resolution of the optical and X-ray data, then the evaporative time scale will be long compared with the age of the remnant, and evaporation should be an ongoing process throughout. The X-ray brightness should increase toward the center of the Loop, at least for a distance of a parsec of so. This is just the opposite of what is observed when comparing XA and HPD's region III. Region III is the clearest example of a largely engulfed cloud or cloud complex in our field, yet it does not show up as an X-ray enhancement.

d) A Nonevaporative Model

In this section we will begin with the "large cloud" view and consider what happens to the X-ray emission as a result of higher preshock densities and dynamical compression of the hot plasma behind the blast wave.

i) *Higher Preshock Density*

In popular models of the ISM an enhancement of the diffuse medium in the vicinity of the cloud cores could be expected as warm diffuse envelopes form around clouds exposed to the interstellar UV flux and hot coronal gas (e.g., McKee and Ostriker 1977). (Although the time taken for these envelopes to form completely may be longer than the average time between "stripping" by shocks [e.g., Heathcote and Brand 1983], there is still expected to be some envelope present for the shock to strip.) A denser than average intercloud medium in the vicinity of dense clouds provides a straightforward explanation of the large-scale correlation between optical and X-ray emission. So

long as the temperature behind the blast wave remains high enough, a denser preshock intercloud medium will always increase the X-ray emissivity behind the blast wave more efficiently than trying to evaporate the same amount of material from clouds. This picture leads directly to the observed "pancakes" with optical cores and extended wings of brighter than average X-ray emission.

Variations in the density of the preshock "intercloud" medium can account for regions of bright X-rays not associated with optical emission, whereas evaporation requires the presence of the dense clouds which would be seen at optical wavelengths (unless the clouds evaporated completely before cooling). A denser "intercloud" medium could also explain the association of X-ray emission with indentations in the Loop. The breakout in the southwest may be an example of the complementary situation where a lower than average density has resulted in faint X-ray emission and a protrusion of the shell.

There is independent evidence in favor of a preexisting intermediate density medium. Such a medium has been proposed by Raymond *et al.* (1980*b*, 1983) to account for Balmer-line filaments coincident with the edge of the X-ray shell (although the shock velocity they obtained may not be high enough for X-ray emission). A low-resolution ($\sim 2'$) broad-band ultraviolet (1300–1800 Å) image of the Cygnus Loop obtained with the FAUST instrument aboard *Spacelab 1* (Bixler *et al.* 1984) shows faint emission from the region of the northeast X-ray limb (J. Bixler 1984, private communication). We suspect that this will also be found to require a postblast temperature there somewhat lower than 2×10^6 K and a higher than average density.

ii) *Rapid Deceleration of the Blast Wave*

As a spherically symmetric blast wave expands into a homogeneous medium, it sweeps up additional material and decelerates. The deceleration produces an effective "gravity" in the frame of the shock which gives rise to the drop in pressure behind the blast wave toward the center of the remnant, as in the standard Sedov solution. If there is a steep positive gradient in the density of the preshock medium, the blast wave decelerates more quickly, the effective "gravity" in the frame of the shock increases, and the magnitude of the rise in pressure toward the edge of the shell grows as its "scale height" decreases. An example of this can be found in Cox and Franco (1981), who consider Sedov's (1959) self-similar blast wave solutions for power-law density distributions. In the case where $n_0 \propto R^4$, for example, the pressure rise occurs over the outer tenth of the radius of the remnant, rather than over the outer third of the remnant as it does in the case of a flat density distribution.

The degree to which a density gradient will affect the pressure can be estimated by calculating the pressure required to decelerate the material in the shell. Assuming that the preshock density has been constant throughout the expansion of the remnant, the mass per unit area in the shell will be about $R\rho_0/3$. The material in the shell must decelerate at three-fourths the rate of deceleration of the blast wave, which requires a pressure differential

$$\delta\rho \approx \tfrac{1}{4} R \rho_0 \dot{v}_b \, .$$

This "deceleration pressure" as a fraction of the pressure behind a blast wave moving into a medium of density ρ_0 with a velocity v_{b0} is

$$\frac{\delta p}{p(v_{b0})} \approx \frac{1}{3} R \frac{\dot{v}_b}{v_{b0}^2} = \frac{1}{2} \frac{\dot{v}_b}{\dot{v}_b(\text{Sedov, homogeneous})} \, .$$

This simple treatment can overestimate δp because it is not necessary to slow the entire shell at once. The increase in pressure throughout the thickness of the shell will occur roughly in the sound crossing time for the thickness of the shell ($\sim 0.15 R/v_b \approx 7500$ years for the typical Cygnus Loop model). A decrease from 400 km s^{-1} (the "average" blast wave velocity) to 200 km s^{-1} (about the minimum velocity necessary for X-ray production) in a crossing time gives $\delta p/p(v_{b0}) \approx 1$. The lower temperature and higher pressure require a larger n and hence brighter X-ray emission.

These numbers are highly uncertain, although the conclusion that the pressure enhancement at the edge derived from the momentum of the shell can be comparable to the original pressure is probably secure. The magnitude of the result is consistent with the effect of momentum conservation in the Sedov solution. Detailed models are needed for more rigorous evaluation of the effects of gradients in preshock conditions on the X-ray emission and overall dynamics.

Rapid deceleration of the shell will affect X-ray emission in two ways. First, there will be inertial compression of the hot previously shocked material behind the blast wave as it slows down and part of its momentum is converted to pressure. Second, the increase in pressure will further enhance the effects of a higher preshock density discussed above by driving a shock with a greater than expected velocity into the denser medium. The result is that a higher density in the X-ray emitting zone is achieved ($4n_0$) with less of a temperature drop than expected from pressure equilibrium. A substantial increase in X-ray emission is thus possible.

It should be noted that the conditions leading to bright X-ray emission are only *slightly* less extreme than those leading to an even higher density, lower temperatures, and radiative shocks. Thus a close association is expected between bright X-ray emission, coronal line emission, UV line emission, and optical complexes just from the sensitivity of the emission behind the blast wave to small changes in the preshock density. Near the intersection of the blast wave and a cloud, the X-ray emissivity will increase with density until it dies very abruptly, just before the onset of optical emission. This might account for the location of XB just beyond the tip of an [O III] arc.

iii) *Reflected and Bow Shocks*

The encounter of a blast wave with a cloud has been discussed by a number of authors (e.g., McKee and Cowie 1975; Spitzer 1982; Heathcote and Brand 1983). The basic assumptions in most treatments of such encounters are that the clouds are spherical, the edges of the clouds are abrupt, and the clouds are sufficiently dense to be considered incompressible for the purposes of calculation of the reflected shock. (Reflected shocks could also form around "bumps" on the surface of a larger cloud, as perhaps is the case for the "trunk" in XA.) Figure 7 shows the geometry of the encounter at two epochs. The notation used is standard, with 0, 1, 2, and c denoting conditions ahead of the blast, behind the blast, behind the reflected shock, and in the cloud, respectively.

The very early stages of the encounter between the shock and the cloud are essentially the same as a normal encounter with a rigid plane. Assuming $\gamma = 5/3$, Courant and Friedrichs (1948) find for this case that $p_2/p_1 = 6$. Depending on the Mach number of the flow behind the blast wave with respect to the cloud (and hence on the Mach number of the blast wave), the reflected shock either dissipates as an acoustic wave or becomes a standing bow shock (which also dissipates eventually). Since the transition between the two cases occurs

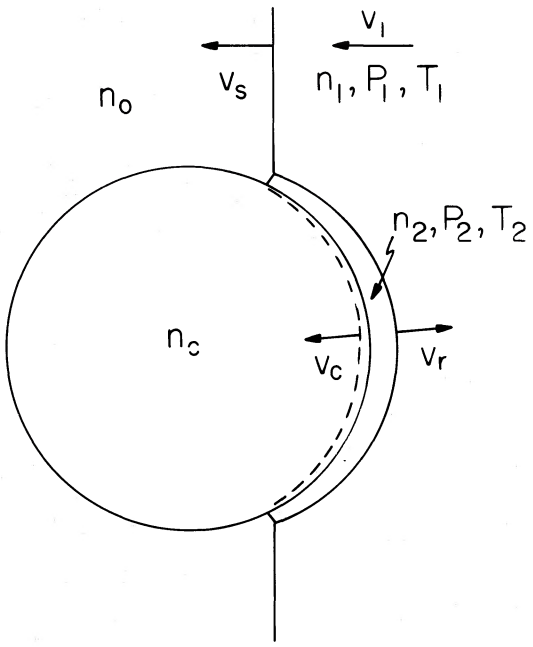

FIG. 7*a*

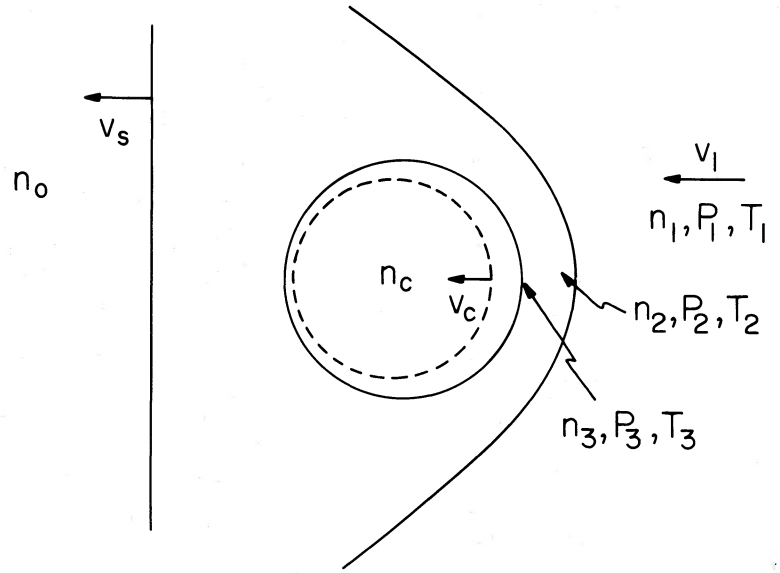

FIG. 7*b*

FIG. 7.—Sketches showing the geometry and labeling for an encounter between a blast wave and a spherical cloud. (*a*) The reflected shock is shown shortly after its formation, before the cloud has been passed by the blast wave. (It is suggested in the text that this is the situation at the bright X-ray region XA.) (*b*) The steady state bow shock around the cloud is shown sitting in the flow behind the adiabatic blast wave. The standard subscripts 0, 1, 2, and *c* refer to conditions ahead of the blast wave, behind the blast wave, behind the reflected shock, and in the cloud, respectively. The subscript 3 refers to conditions at the stagnation point at the nose of the cloud. X-ray emission should increase across the reflected shock, where the material behind the blast wave, already heated to X-ray temperatures, is subjected to further heating and compression.

at M_s (the Mach number of the blast wave) = 2.76 (e.g., Spitzer 1982) it is likely that most of the reflected shocks do not quickly dissipate. The pressure p_3 at the stagnation point at the nose of the cloud will be somewhat lower than the pressure immediately behind the bow shock. The stagnation pressure has been calculated by McKee and Cowie (1975). Table 2 (adapted from Spitzer 1982) lists properties in the regions of interest as a function of the Mach number of the blast wave.

In the case of blast wave propagation through a cloudy medium, the X-ray emission should be exceptionally strong behind the reflected and bow shocks, where material that has already been heated to X-ray temperatures by the blast wave is subjected to additional heating and compression. Since the blast wave of the Cygnus Loop is in the strong shock limit, p_2/p_1 will approach 6 at its peak value (and across the entire face of the reflected shock immediately after the encounter). This is enough to explain the high pressure inferred for XA. For this case, the Mach number of the reflected shock M_r is equal to 2.24, $\rho_2/\rho_1 = 2.5$, and $T_2/T_1 = 2.4$. The density enhancement alone gives an increase in the volume emissivity

TABLE 2

PROPERTIES ACROSS BOW SHOCKS AROUND SPHERICAL CLOUDS

PROPERTY	M_s = 1.00	2.00	5.00	∞
M_r	1.00	1.65	2.11	2.24
p_2/p_1	1.00	3.14	5.29	6.00
ρ_2/ρ_1	1.00	1.90	2.39	2.50
T_2/T_1	1.00	1.66	2.22	2.41
p_3/p_1	1.00	1.59	2.72	3.15

of a factor of 6.25 over the material behind the adiabatic blast. Because of the steep ($T^{5/2}$) temperature dependence of evaporative mass loss, evaporation into region 2 (Fig. 7) would, in the absence of an adverse magnetic field configuration, also be enhanced (initially by a factor of >5) and could further contribute to the density and thus to the X-ray emissivity.

If the medium around the cloud were already somewhat denser than average (as discussed in § IV*d*[i]), then the enhancement over the average X-ray emissivity will be larger. For example, if the material behind the blast wave in the vicinity of the cloud were about twice as dense and half as hot as average, then the reflected shock would heat it up to about the "average" temperature of 2×10^6 K. The density behind the reflected shock would be 6 times the average behind the blast wave, and the volume emissivity would be 36 times as great. If the pressure in region 1 were already higher than average (as discussed in § IV*d*[ii]), then X-ray temperatures would be maintained at yet higher densities, resulting in an even greater enhancement of the X-ray emissivity over the average value behind the adiabatic blast wave.

The early phase during which $p_2/p_1 = 6$ across the face of the cloud will last a time comparable to that taken by the blast wave to pass the cloud. If the clouds are large, this will be long compared to a cooling time (for $R_c = 1$ pc and $v_b = 400$ km s^{-1}, $R_c/v_b \approx 2.5 \times 10^3$ years), so this situation should still apply to regions such as XA where much of the optical emission is younger than a cooling time (certainly $< 10^3$ years). In § III*d* we also argued that on the north side of the region we can identify the point at which the blast wave is attached to the cloud.

The geometry and the nature of the emission at XA are consistent with a zone of emission behind a reflected shock. The peak X-ray emission occurs at the nose of the cloud (where the pressure is the greatest) and tapers off to the north as the edge of the emission turns east (i.e., where the blast wave wraps around the edge of the cloud and the pressure needed to divert the flow is lower). Early on, the reflected shock has a velocity of $v_s/2$ with respect to the cloud (e.g., Spitzer 1982). The apparent thickness of the zone of X-ray emission ($\lesssim 0.2$ pc) requires that the plane of the unimpeded blast wave be $\lesssim 0.4$ pc east of the optical emission. This is about equal to the east-west separation (~ 0.35 pc) between the optical emission at XA and the point at the end of the arc between XA and XB where the blast wave currently seems to intersect the cloud. The larger indentation in the X-ray shell surrounding XA must be due largely to the encounter with the denser envelope around the cloud. The time since the encounter inferred from the geometry (0.35 pc/400 km s^{-1} $\lesssim$ 900 years) is somewhat longer than expected on the basis of the emission type, although not disturbingly so. The geometry is not perfectly known, so if 0.07 pc is taken as the thickness for the zone behind the reflected shock, then the inferred time since the encounter drops to ~ 350 years. Also, since the time needed for the gas to radiate its thermal energy varies as $T/n \propto p/n^2$, the higher pressure driving the radiative shocks will result in a longer cooling time than that estimated in § IV*c*(ii)(2). Thus 1000 years for a time since encounter is possible. If the bright zone is approximately tangential to the line of sight, then the line-of-sight depth of the thin emitting region will be $\sim R_c$.

After the blast wave has passed, the reflected shock will move away from the cloud, form a "steady state" bow shock for a time, and eventually dissipate. If the stagnation pressure p_3 is taken as characteristic of the bow shock region, then $p_3/p_1 \approx 2$, and the X-ray emissivity will be no more than a factor of 4 higher than average. (It would probably be a good deal lower owing to the decreasing density in the post–blast wave flow with increasing distance behind the blast wave.) This could explain the lack of strong X-ray emission from HPD's much older region III. The shape of the locus of optical emission also suggests a pointed intrusion into the shell. This shape (which could result from the action of the shock itself) would not impede the flow as much as a blunt cloud like the one at XA, and hence would not have as much of an effect on the X-ray emission. A similar argument can account for the lack of X-ray emission associated with the horizontal bar across the center of the field.

The enhancement of X-ray emission expected as a result of strong inertial compression needed to divert the hot flow around large clouds is adequate to account for exceptionally bright regions such as XA. This also satisfies the morphological characteristics of the X-ray emission and its relation to the optical structure. Applied to the smaller irregularity represented by the optical knots at the western end of the "trunk" in XA, it may also account for the associated X-ray bright spot to the west. There, however, the role of thermal conduction is more ambiguous.

The details of the geometry of the cloud and the flow around it provide other opportunities for inertial compression of the hot plasma. Calculations of radiation-driven implosions of clouds by Sandford, Whitaker, and Klein (1982, 1983) show many "hot spots" where there are significant transient increases in the pressure. A similar phenomenon might be expected to occur in the present case. Focusing of shocks or funneling of the hot flow may also occur. As noted above, the brightest knot in XA is located at an exterior corner in the X-ray contours above about 0.05 counts arcmin^{-2} s^{-1}. It is a region of V-shaped [O III] filaments and may be at the interior corner of an L-shaped cloud. This knot may arise from funneling of the flow into the corner, or from intersection of the reflected shocks.

e) Coronal Line Emission

The X-ray emission has a characteristic temperature of 2×10^6 K ($10^{6.3}$), while the optical filaments follow shocks with temperatures $\sim(1\text{–}3) \times 10^5$ K. In collisional equilibrium, Fe^{+9} peaks in abundance between $10^{5.9}$ and $10^{6.1}$ K (Arnaud and Rothenflug 1985), while Fe^{+13} peaks just below $10^{6.3}$ K. Since both the optical and X-ray emission are found in close association, one naturally expects the intermediate conditions yielding iron coronal lines to be present as well. This expectation must be tempered by considerations of nonequilibrium ionization structure and the particular model details used to describe the optical and X-ray emission in each small region.

In the general region of XA, avoiding the brighter spots, the electron density is probably ~ 4 cm^{-3} in the X-ray emitting gas, the temperature is 2×10^6 K, and the pressure p/k is $2n_e T \approx 16 \times 10^6$ cm^{-3} K. We have argued that this is probably due to a shock reflected off the cloud along the escarpment and that the encounter began about 1000 years ago. For such a reflected shock the original preshock density just outside the cloud would have been a factor of 10 lower, 0.4 cm^{-3}, and the original postshock pressure (before reflection) a factor of 6 lower, 3×10^6 cm^{-3} K. The cloud shock is probably driven, in this case, by the same pressure as exists in the X-ray region, so that for a postshock temperature of T_c behind the cloud shock and initial cloud density n_{c0} we have $T_c \approx 2 \times 10^6$ cm^{-3} K$/n_{c0}$. Thus a cloud density of order 10 cm^{-3} will lead to conditions for a radiative shock. We infer that the initial density contrast between the cloud and its western intercloud medium was a factor of roughly 25.

If the idealized picture held in detail, with a reflected shock region with $T \approx 2 \times 10^6$ K and a cloud shock region with $T \lesssim 2 \times 10^5$ K, then one might in collisional equilibrium expect to see [Fe XIV] but not [Fe X], the latter being favored in an isolated temperature regime around 10^6 K. Nonequilibrium ionization does not change this conclusion significantly. At 2×10^6 K, the ionization rate coefficients for Fe^{+8} to Fe^{+13} in units of 10^{-10} cm^3 s^{-1} are roughly 8, 5, 4, 2, 1.3, and 0.7. An electron density of 4 cm^{-3} implies ionization rates, respectively, of roughly 100, 60, 50, 25, 15, and 8 per 10^3 years. Thus, the lifetimes of Fe^{-9} and Fe^{+13} are roughly 16 and 125 years in the X-ray emitting region. We expect the average Fe^{+9} and Fe^{+13} concentrations in the region to be less than or of order 0.02 and 0.13, respectively, given the 1000 year accumulation of material in the reflected shock region.

In the region just interior to (west of) the reflected shock, however, the density should still be of order 1.5 cm^{-3} and the temperature still nearly 10^6 K. This should be a prime location for the observation of [Fe X]. Its presence or absence may, however, be quite sensitive to the specific temperature (and therefore density) structure of the medium. At 10^6 K the ionization rate coefficients (Arnaud and Rothenflug 1985) for Fe^{+8} and Fe^{+9} are down to 1.7 and 0.9×10^{-10} cm^3 s^{-1}, so that at $n_e \approx 1.5$ cm^{-3} the rates would be 8 and 4 ionizations per 10^3 years. Since this material would have been shocked by the blast wave 1500 years ago, Fe^{+9} should be close to its equilibrium abundance.

This picture is greatly complicated by details. We have seen that [Fe X] should be found behind the main blast wave when it encounters densities of order 0.4 cm^{-3}, but with an ionization structure lagging by about 300 years while Fe^{+8} is ionized. [Fe XIV], however, requires a factor of 2 higher temperature. Except in highly transient conditions, or in situations with a stable gradient in temperature (e.g., evaporation boundaries of clouds), one would not expect a detailed correlation between emission of the two coronal ions or between [Fe X] and soft X-ray emission on a scale smaller than 0.2 pc. In a complex region the two coronal lines should usually be found neighboring but not in coincidence, and their relative brightness should correlate well with the local X-ray temperature.

These expectations can be tested in part for the vicinity of the escarpment by comparing the optical and X-ray data in Figure 5 with the [Fe X] λ6374 map of Teske and Kirshner (1985). Their Figure 2 shows [Fe X] contours superposed on the red POSS print. The region of the brightest X-ray knot is not exceptionally bright in [Fe X], nor is the X-ray peak in the northeastern part of Figure 5. This second knot is quite interesting in comparison with the [Fe X] map, however. It is bordered on the north, west, and south by bright [Fe X] emission (crosshatched regions in Fig. 2 of Teske and Kirshner 1985), but sits in a local minimum of [Fe X]. Likewise, the crosshatched regions of bright [Fe X] (including the region south of the bright optical knots in the center of our Fig. 5) all coincide with local minima in the X-ray image.

It is clear that the structure is irregular on the scale of the X-ray bright region (0.3 pc) and that the sensitivity of [Fe X] to temperature variations makes its brightness particularly sensitive to irregularities. These are very low contrast density irregularities, however, and we discourage reference to them as clouds. They involve modest differentials in intercloud medium density (leading to only factors of 2 in postshock temperature) and irregularity in the boundary of a much larger scale cloud. The density differential between clouds and the intercloud medium, on the other hand, exceeds an order of magnitude near the clouds and is 2 orders of magnitude between the clouds and the intercloud medium far from clouds.

In comparing our interpretation of the [Fe X] emission with that of Teske and Kirshner (1985), we find complete concurrence regarding the densities, temperatures, and times involved, and disagreement over the origin of the material and elevated pressures. There are irregularities on the scales they discuss, but they are just that—modest irregularities in a larger scale structure. These preexisting irregularities, together with the sensitivity of [Fe X] to temperature, provide the structure seen in the [Fe X] map, with no need for thermal evaporation. The [Fe X] emission simply traces the presence of 10^6 K gas in a region where the presence of both bright optical and X-ray emission signify a range of conditions with temperatures varying from $< 10^5$ to 2×10^6 K.

f) The ISM around the Cygnus Loop

We have concluded that the brightest X-ray emission around the rim of the Cygnus Loop is due to the presence of large clouds and extended regions of higher than average density. It might still be possible to claim that the emission from the "unbrightened" portion of the shell is due to evaporation of clouds behind a faster shock, but the smooth nature of the X-ray shell would require that a model similar to the "small cloudlet picture" be invoked for the low-density phase. A much more plausible explanation is that most of the shell is expanding into an ionized medium with a fairly uniform density of ~ 0.1 cm^{-3} (similar to, but somewhat less dense than, the "warm ionized medium" from McKee and Ostriker 1977). Embedded in this medium are H I clouds much like standard diffuse (and perhaps also large) clouds discussed by Spitzer (1978, 1985), as well as a less dense, partially neutral component similar to the "warm neutral medium" from McKee and Ostriker (1977), the mechanically heated phase of Cox (1981), or the "not strongly absorbing" material from the 21 cm study of Payne, Salpeter, and Terzian (1983). The only evidence for the presence of a very diffuse "hot ionized medium" around the exterior of the Loop is the breakout in the south. As noted by KKPL, this looks much as expected for a breakthrough into a "tunnel" as described by Cox and Smith (1974).

The ISM around that Cygnus Loop does not appear to be the McKee and Ostriker ISM. Nor is the description of the Cygnus Loop in the preceding sections that of an evaporative SNR as described by McKee and Cowie (1975) and Cowie,

McKee, and Ostriker (1981). We find that the inhomogeneity of the ISM affects the radiative cooling of the interior of the remnant in ways not addressed by the models. We also find a lack of observational evidence to suggest that evaporation is as important a process as assumed by the models (at least for the Cygnus Loop).

V. SUMMARY

We have presented a comparison at a resolution of 17″ between optical emission from [O III] and [S II] and the thermal X-ray emission for a field on the southeast edge of the Cygnus Loop SNR. The optical lines used represent emission from two ionic species found in extreme portions of the cooling regions behind radiative shocks. As expected (given the fact that the emission comes from physically different media), no one-to-one correlation between optical and X-ray emission exists across the field. Two extended regions of bright X-ray emission are associated with optical emission, however. The edge of the region of brightest X-ray emission is coincident with the leading edge of the optical emission to within the alignment uncertainty and resolution of the data over a length of several minutes of arc. In this region the spatial relationship between the X-ray and the optical emission is consistent with X-ray emission coming from a thin ($\lesssim$0.2 pc thick) zone located immediately behind the much thinner, sheetlike locus of optical emission. At this location the data do not suggest that the optical filaments have been engulfed by the blast wave. We believe that this conclusion can be generalized to most of the optical emission in the Loop.

Several possible explanations for the brighter than average X-ray emission in the vicinity of the optical emission are discussed. Cloud evaporation (which has been favored by some authors for explaining the gross correlation between optical and X-ray emission in the Cygnus Loop and other similar SNRs) has a number of problems: (1) The contrast between regions of enhanced and unenhanced emission is too great to be easily explained by evaporation alone. (2) The small clouds required by some formulations of the evaporative picture do not lead to the observed optical morphology. (3) The detailed coincidence of X-ray and optical emission along a parsec-long edge is difficult to explain, owing to differences in the time scales for evaporation and cooling. (4) There is no X-ray enhancement associated with a large cloud which should have had time to undergo significant evaporation. (5) There is strong X-ray emission from regions (such as the X-ray bright northeast limb) where the optical data do not show the presence of clouds.

The physical picture which we find best fits the data is a multiphased medium with large clouds ($R_c \geq 1$ pc, with sizes or associations to the "facet" size of $\sim$20 pc) immersed in a lower density "intercloud" medium. The latter is somewhat denser near the clouds ($n \approx 0.5$ cm^{-3}) than elsewhere ($n \approx 0.1$). (With the possible exception of the breakout in the south, this intercloud medium is *not* the "hot ionized medium" which is the dominant phase of the McKee and Ostriker ISM. While one should not necessarily expect the Loop environment to be representative of the ISM as a whole, given the importance of SNRs in models such as theirs it is significant that the Cygnus Loop seems not to be evolving in the way predicted.) Bright X-ray emission not locally associated with optical emission is explained by the extension of the denser intercloud medium beyond the cloudy regions. The X-ray emission from such regions will be brighter because of the higher preshock density, and will be maintained to higher densities by pressure enhancement via inertial compression associated with deceleration of the blast wave as it runs up the density gradient. These mechanisms also apply in the immediate vicinity of the optical emission, where reflected shocks behind large clouds can account for the detailed coincidence of the brightest X-ray emission with optical features.

We feel secure in the conclusion that the "small cloudlet" picture of the Cygnus Loop is not viable. The discussion of evaporation as it applies to large clouds could be altered by time-dependent calculations of the early phases of evaporation. Regions of higher than average X-ray emissivity *will* occur as a result of variations in the preshock intercloud density and dynamical compression of material behind the blast wave. Even in the absence of evaporation these effects appear to be adequate to explain the higher pressure and volume emissivity inferred in § III for the bright X-ray regions. More work, both observational and theoretical, is needed to clarify the relative importance of these effects and thermal evaporation for the Cygnus Loop and other SNRs.

The authors wish to thank William Ku for providing the X-ray data presented here and for a preprint of the work by him and his collaborators on the Cygnus Loop. We acknowledge helpful discussions with J. C. Raymond, R. A. R. Parker, and R. J. Dufour. This work represents a portion of the research conducted by J. J. H. toward completion of a Ph.D. in space physics and astronomy at Rice University. This research was supported in part by National Aeronautics and Space Administration contracts NAS9-15940 and NAS9-16596 and by the National Science Foundation under grant AST 84-15142. J. J. H. acknowledges the support of a NSF Graduate Fellowship during a period including a portion of this research, and also expresses gratitude to the ARCS Foundation for very generous awards over the last three years. D. P. C. is grateful for the hospitality of Rice University during the period of this effort.

REFERENCES

Arnaud, M., and Rothenflug, R. 1985, *Astr. Ap. Suppl.*, in press.
Ballet, J., Arnaud, M., and Rotherflug, R. 1984, *Astr. Ap.*, **133**, 357.
Bixler, J., Bowyer, S., Deharveng, J. M., Courtès, G., Malina, R., Martin, C., and Lampton, M. 1984, *Science*, **225**, 184.
Courant, R., and Friedrichs, K. O. 1948, *Supersonic Flow and Shock Waves* (New York: Interscience), pp. 152–154.
Cowie, L. L., and McKee, C. F. 1977, *Ap. J.*, **211**, 135.
Cowie, L. L., McKee, C. F., and Ostriker, J. P. 1981, *Ap. J.*, **247**, 908.
Cox, D. P. 1972, *Ap. J.*, **178**, 169.
———. 1979, *Ap. J.*, **234**, 863.
———. 1981, *Ap. J.*, **245**, 534.
Cox, D. P., and Franco, J. 1981, *Ap. J.*, **251**, 687.
Cox, D. P., and Smith, B. W. 1974, *Ap. J. (Letters)*, **189**, L105.
DeNoyer, L. K. 1975, *Ap. J.*, **196**, 479.
Dickel, J. R., and Willis, A. G. 1980, *Astr. Ap.*, **85**, 55.
Draine, B. T., and Giuliani, J. L., Jr. 1984, *Ap. J.*, **281**, 690.
Falle, S. A. E. G., and Garlick, A. R. 1982, *M.N.R.A.S.*, **201**, 635.
Fesen, R. A., Blair, W. P., and Kirshner, R. P. 1982, *Ap. J.*, **262**, 171.
Gull, T. R., Parker, R. A. R., and Kirshner, R. P. 1977, in *Supernovae*, ed. D. N. Schramm (Dordrecht: Reidel), p. 71.
Heathcote, S. R., and Brand, P. W. J. L. 1983, *M.N.R.A.S.*, **203**, 67.
Henbest, N., and Marten, M. 1983, *The New Astronomy* (Cambridge: Cambridge University Press).
Hester, J. J. 1985, in preparation.
Hester, J. J., Parker, R. A. R., and Dufour, R. J. 1983, *Ap. J.*, **273**, 219 (HPD).
Kahn, S. M., Harnden, F. R., Jr., Seward, F. D., and Gorenstein, P. 1984, preprint.
Kato, T. 1976, *Ap. J. Suppl.*, **30**, 397.

Ku, W. H.-M., Kahn, S. M., Pisarski, R., and Long, K. S. 1984, *Ap. J.*, **278**, 615 (KKPL).
Lucke, R. L., Woodgate, B. E., Gull, T. R., and Socker, D. G. 1980, *Ap. J.*, **235**, 882.
Mathewson, D. S., Ford, V. L., Dopita, M. A., Tuohy, I. R., Long, K. S., and Helfand, D. J. 1983, *Ap. J. Suppl.*, **51**, 345.
Mauche, C., and Gorenstein, P. 1984, *Bull. AAS*, **16**, 926.
McCray, R., and Snow, T. P. 1979, *Ann. Rev. Astr. Ap.*, **17**, 213.
McKee, C. F., and Cowie, L. L. 1975, *Ap. J.*, **195**, 715.
McKee, C. F., and Ostriker, J. P. 1977, *Ap. J.*, **218**, 148.
Miller, J. S. 1974, *Ap. J.*, **189**, 239.
Minkowski, R. 1958, *Rev. Mod. Phys.*, **30**, 1048.
Parker, R. A. R. 1967, *Ap. J.*, **149**, 363.
Payne, H. E., Salpeter, E. E., and Terzian, Y. 1983, *Ap. J.*, **272**, 540.
Poveda, A., and Woltjer, L. 1968, *A.J.*, **73**, 65.
Rappaport, S., Doxsey, R., Solinger, A., and Borken, R. 1974, *Ap. J.*, **194**, 329.
Rappaport, S., Petre, R., Kayat, M. A., Evans, K. D., Smith, G. C., and Levine, A. 1979, *Ap. J.*, **227**, 285.
Raymond, J. C., Black, J. H., Dupree, A. K., Hartmann, L., and Wolff, R. S. 1980*a*, *Ap. J.*, **238**, 881.
Raymond, J. C., Blair, W. P., Fesen, R. A., and Gull, T. R. 1983, *Ap. J.*, **275**, 636.
Raymond, J. C., Davis, M., Gull, T. R., and Parker, R. A. R. 1980*b*, *Ap. J. (Letters)*, **238**, L21.
Raymond, J. C., and Smith, B. W. 1977, *Ap. J. Suppl.*, **35**, 419.
Sandford, M. T., II, Whitaker, R. W., and Klein, R. I. 1982, *Ap. J.*, **260**, 183.
———. 1983, *Ap. J.*, **282**, 178.
Sedov, L. I. 1959, *Similarity and Dimensional Methods in Mechanics* (New York: Academic).
Shull, P., Jr., Dyson, J. E., Kahn, F. D., and West, K. 1984, preprint.
Smith, M. D., and Dickel, J. R. 1983, *Ap. J.*, **265**, 272.
Spitzer, L., Jr. 1978, *Physical Processes in the Interstellar Medium* (New York: Wiley).
———. 1982, *Ap. J.*, **262**, 315.
———. 1985, *Ap. J. (Letters)*, **290**, L21.
Straka, W. C. 1984, preprint.
Straka, W. C., Dickel, J. R., Blair, W. P., and Fesen, R. A. 1983, *Bull. AAS*, **15**, 929.
Teske, R. G., and Kirshner, R. P. 1985, *Ap. J.*, **292**, 22.
Treffers, R. R. 1981, *Ap. J. (Letters)*, **250**, L213.
Tucker, W. 1971, *Science*, **172**, 372.
Tucker, W. H., and Koren, M. 1971, *Ap. J.*, **168**, 283.
van der Laan, H. 1962*a*, *M.N.R.A.S.*, **124**, 125.
———. 1962*b*, *M.N.R.A.S.*, **124**, 179.
Woodgate, B. E., Kirshner, R. P., and Balon, R. J. 1977, *Ap. J. (Letters)*, **218**, L129.

DONALD P. COX: Department of Physics, University of Wisconsin, 1150 University Avenue, Madison, WI 53706

J. JEFF HESTER: Department of Planetary Science, Mail Stop 170-25, California Institute of Technology, Pasadena, CA 91125